1989

NMR studies of amorphous silicon and aluminosilicate glass

William Wel-Lin Shao
Iowa State University

Order Number 9014953

NMR studies of amorphous silicon and aluminosilicate glass

Shao, William Wel-Lin, Ph.D.

Iowa State University, 1989

U·M·I
300 N. Zeeb Rd.
Ann Arbor, MI 48106

NMR studies of amorphous silicon and aluminosilicate glass

by

William Wei-Lin Shao

A Dissertation Submitted to the
Graduate Faculty in Partial Fulfillment of the
Requirements for the Degree of
DOCTOR OF PHILOSOPHY

Department: Chemistry
Major: Physical Chemistry

Approved:

Signature was redacted for privacy.
In Charge of Major Work

Signature was redacted for privacy.
For the Major Department

Signature was redacted for privacy.
For the Graduate College

Iowa State University
Ames, Iowa

1989

TABLE OF CONTENTS

LIST OF FIGURES

PART ONE. NMR STUDIES OF ZERODUR

PART TWO. NMR STUDIES OF AMORPHOUS SILICON

LIST OF TABLES

INTRODUCTION

There exists a wide range of different amorphous solids each with its own unique structure. Since amorphism is a metastable state of matter, their structures depend not only on composition but also on thermal history. The only aspect these materials have in common is their complete lack of long range order.

The field of amorphous solids is an area not amenable to most of the conventional theoretical techniques of solid-state physics. For many years amorphous solids were difficult systems to describe as there is no ideal structure which can be accepted with complete confidence and can be used as a starting point for a determination of the concentration of various types of defects and impurities as deviations from the ideal structure as in the situation of a crystal. The word "amorphous" means "structureless", hence to seek a reproducible measurement on such a material is perhaps not totally meaningful.

In the past two decades Nuclear Magnetic Resonance (NMR) spectroscopy has became one of the most powerful techniques for investigating the magnetic and electronic interactions present in a wide variety of materials. In particular, the technique of magic angle spinning (MAS) NMR has been used to obtain high-resolution spectra of solids. The broadening effect of the dipole-dipole interaction and the anisotropic part of the chemical shielding tensor is removed by rapid

rotation of sample at the "magic angle" (54.7°) with respect to the magnetic field. Also the broadening due to electric field gradients on quadrupolar nuclei is reduced.

In this thesis, the capabilities of NMR were utilized to probe the local structure and local ordering in an aluminosilicate glass sample and an amorphous Si sample.

PART ONE. NMR STUDIES OF ZERODUR

INTRODUCTION

Aluminosilicate glasses have been industrially produced and widely used in daily life for hundreds of years. The chemical and physical properties of aluminosilicates are of commercial and theoretical interest. A detailed knowledge of the structure of these materials is needed to better understand their properties and to improve them to produce new glasses. A glass is presumed to be the quenched equivalent of a melt. That is, the structure of the melts at the glass transition temperature is retained in the glass state, except that the molecular motions characterizing the liquid state are no longer present. Thermodynamically, a melt is substantially different from the glass because of the dynamics present in the molten state.

NMR spectroscopy which is very sensitive to the local electron environments surrounding nonzero spin nuclei[1] has proven invaluable in determination of silicon-aluminum local ordering in aluminosilicate glasses[2]. X-ray diffraction techniques have difficulty, even in single crystals, distinguishing aluminum atoms from silicon atoms because their atomic radii are almost identical and they can occupy the same structural positions. The only differentiating feature is that the Al-O bond length is slightly longer than that of Si-O. This difference is not possible to distinguish in many aluminosilicate structures. Both ^{29}Si and ^{27}Al NMR have been of great value in

investigations of aqueous, crystalline, glassy and molten aluminosilicate structures. In particular, the technique of magic angle spinning (MAS) NMR has been used to obtain high-resolution spectra of solids. The broadening effect of the dipole-dipole interaction and the anisotropic part of the chemical shielding tensor is removed by rapid rotation of sample at the "magic angle" (54.7°) with respect to the magnetic field[3]. Also the broadening of the quadrupole interaction is reduced. In this part of work, ^{29}SI and ^{27}Al MAS NMR spectra were measured and it was found that two different regions with different local ordering exist in the glassy ceramic sample.

LITERATURE REVIEW

Structure of Silicate and Aluminosilicate Glasses

The simplest of the silicate glasses is vitreous silica, SiO_2. The study of its molecular structure has been fundamental to understanding the structure of other silicates.

In 1926, Goldschmidt[4] recognized that the oxygen ions were tetrahedrally arranged around silicon ions in silicates.

In all crystalline silicates the coordination number of silicon-to-oxygen ions is four, and the silicon-oxygen tetrahedron is the basic building block for silicate structure. These tetrahedra can be attached to none, one, two, three and four other tetrahedra by sharing corner oxygen atoms, depending on the concentration of other oxides present.

In 1932, Zachariasen[5] proposed an idealized model, called the continuous random-network model (CRN), for the structure of covalently bonded amorphous solids. According to this model, each Si atom is covalently bonded to four neighboring O atoms in an approximately tetrahedral arrangement, and each O atom is covalently bonded to two neighboring Si atoms. The three-dimensional networks are formed by the union of these tetrahedra at their corners, sharing the corner O atoms.

Variations in bond angles, not permitted in the crystal, is associated with the loss in long range order and local symmetry.

The radial distribution function (RDF) of vitreous silica was obtained in 1936 by the initial X-ray diffraction study of Warren et al.[6] This result allowed the calculation of interatomic distances directly from the peak positions on the curve. The areas under the peaks give the number of neighboring atoms. The RDF established definitely the tetrahedral silicon-oxygen network. The first peak occurs at 1.62 Å in good agreement with the average silicon-oxygen distance, 1.60 Å, found in various crystalline silicates.[7] The number of oxygens about each silicon calculated from the area of the first peak is four. From the geometry of a tetrahedron, if 1.62 Å is the distance from its center to a corner, the distance from corner to corner will be 2.65 Å. The position of the O-O peak at 2.65 Åindicates that the four oxygens are arranged tetrahedrally about the silicon. Similar work on X-ray diffraction and neutron diffraction study were done by several other researchers, Valekov and Porai-Koshitz (1936), Zarzycki (1957), Carraro and Domenici (1963), and Henninger, Buschert and Heaton (1967). In 1969, Mozzi and Warren[8] confirmed this arrangement using Rh Kα radiation with the method of fluorescence excitation which eliminates the approximations made in earlier work and greatly improves the accuracy of the diffraction results. They also obtained the distribution curve of the silicon-oxygen-silicon bond angle from the third, fourth and fifth peaks. The maximum of the distribution curve is at 144°, with the maximum angle of 180° and the minimum angle of 120°. Almost all the angles are within ±10% of the

maximum. This distribution of bond angles is wide enough to distinguish the structure from a crystalline arrangement, but is rather narrow compared to a completely random distribution of bond angles from 90° to 180°. The structure of vitreous silica is therefore relatively uniform at short range, although there is no order beyond several layers of tetrahedra. All these results are consistent with the random-network model. Histograms calculated from physical models of the structure of vitreous silica, based on a random-network and constructed in various ways[9-11], agree well with the experimental results of Warren and Mozzi. Various properties of vitreous silica calculated from the random-network model are also in accord with experimental results. For example, the spectrum of atomic vibrations as measured by infrared absorption, Raman emission, and in elastic neutron scattering is consistent with the random-network model[12-14].

The crystallite models for the structure of vitreous silica have been advocated in which there are regions of order alternating with connecting regions of disorder. These crystallite models,[15,16] where very small crystalline regions are connected by disordered material, were examined by Warren and Briscoe.[17] They showed that the breadth of the first diffraction peak in vitreous silica required a crystallite size of no larger than 8 Å. At this size the term "crystallite" loses any meaning. Furthermore, vitreous silica showed little low-angle X-ray scattering; any appreciable amount of fine nonuniformities would lead to such scattering.

Other models for the structure of vitreous silica based on regions with structures close to that of quartz[18] or tridymite[19] have been

advocated. These models ignore the distribution of Si-O-Si bond angles deduced from the breadth of the third diffraction peak and also the scattering results of Warren and Briscoe.

Models built up of pentagonal dodecahedra[20,21] require a silicon-oxygen-silicon bond angle of 180°, which are inconsistent with the experimental results of Mozzi and Warren for the distribution of these angles.

Bell and Dean have shown that the configurational entropy of a continuous random-network model of vitreous silica is quite low and is consistent with the experimentally measured entropy.[22] McConnell[23] pointed out that the entropy changes of many order-disorder phase transitions are often only half that expected from completed disorder, due to the short-range order.

Extensive model-building studies of the SiO_2, an idealized three dimensional continuous random network, have been carried out by Bell and Dean[24]. Rules used in building up the network specify the following:[25]

1. Fourfold and twofold coordination for silicon and oxygen, respectively, with complete chemical ordering.
2. Constant bond lengths and O-Si-O bond angles.
3. No dangling bonds in the bulk.
4. A significant spread is permitted in Si-O-Si bond angles.
5. There is no long range order.

The first two prescriptions describe the high degree of short-range order. "Chemical ordering" in condition 1 refers to the strong requirement that each Si atom is covalently bonded to four nearest-

neighbor O atoms and each O atom to two nearest-neighbor Si atoms. In condition 2 not only is the Si-O bond length to be kept constant, but so is the O-Si-O bond angle (at 109.47°). Each SiO_4 unit, consisting of a central silicon bonded to four oxygens, defines the body center and vertices of a regular tetrahedron. All of the quantitative variations present in parameters of the nearest-neighbor configurations are to be assumed by the Si-O-Si bond angles. Since the oxygens are bonded to only two neighbors while the silicons are bonded to four, the angles at the oxygens are much less constrained than those at the silicons. The Si-O-Si bond angles are thus softer than the O-Si-O bond angles, and their variation entails a much smaller energy increase. The mean Si-O-Si bond angle in the structure is about 153°, and the rms $\Delta\theta$ is about 15°. Their model showed that the random network theory of glass structure accounts satisfactorily for the observed X-ray and neutron radial distribution functions of vitreous silica, out to interatomic distances of at least 8 Å. They also suggested that the distribution of bond angles may not be the only factor determining the overall agreement between theoretical and experimental radial distribution functions.

In aluminosilicates, silicon tetrahedra may be replaced with aluminum tetrahedra (AlO_4^{5-}). Substitution of aluminum for silicon in tetrahedra was formerly considered to be entirely random and of infinite extent. But at least in some cases the substitution of aluminum for silicon is not random[26,27] and the fact that the substitution of aluminum for silicon in condensed tetrahedra the maximum substitution is 50% cannot be duly explained. In 1953

Loewenstein[28] pointed out that in crystals of silicates and aluminates the distribution of aluminum in the centers of tetrahedra is not entirely at random. He suggested that whenever two tetrahedra are linked by an oxygen bridge, only one center of them can be occupied by aluminum; the other center must be occupied by silicon or other ion of electrovalence four or more. When two aluminum ions are neighbors to the same oxygen anion, at least one of them must have a coordination number larger than four, that is, five or six, towards oxygen. This is known as Loewenstein's aluminum avoidance principle and is attributed to the fact that the Al-O-Al linkage is thermodynamically less favorable than Al-O-Si or Si-O-Si bonds. In aluminosilicates, the negative charge of the framework which is equal to the number of constituent aluminum atoms is balanced by cations M^{n+}, typically alkali or alkaline earth elements. Aluminum atoms in aluminosilicates not only can be tetrahedrally coordinated by four oxygen atoms but also can occupy a charge balancing or network modifying site which is octahedrally coordinated. In a tectosilicate, each silicate or aluminate tetrahedron is linked, by sharing corner oxygen atoms, to four other tetrahedra.

^{29}Si NMR Studies of Silicates and Aluminosilicates

^{29}Si NMR has proven to be a powerful technique for investigating the local structures of amorphous phases, glasses, and various polycrystalline materials, such as clay and zeolites. These materials

have local ordering which can not be readily determined by single crystal diffraction techniques.

There are several atoms, such as ^{27}Al, ^{29}Si, ^{17}O, which can be used in a NMR study of aluminosilicates. Among these atoms, ^{29}Si is the most useful. It is the primary element used in construction of silicates and aluminosilicates. Because ^{29}Si atoms have spin I=1/2 there is no broadening caused by nuclear quadrupole coupling to electric field gradients. Information obtained from the ^{29}Si NMR spectrum is directly related to the structure of the aluminosilicate under investigation and the local ordering of ^{29}Si atom. Both silicate speciation and geometric factors, such as the Si-O-Si bond angle[29-32], and Si-O bond lengths[33], influence the ^{29}Si chemical shift. Therefore NMR is useful for characterizing several aspects of local silicate structure. The dipole interaction which severely broadens the NMR spectrum lines in some solids can be averaged to be zero and removed by fast MAS. Under MAS, the NMR peak widths are greatly narrowed and the line width of the NMR spectrum mainly reflects the local disordering of Si tetrahedra. As a result the spectral lines are quite well resolved and relatively straightforward to interpret from empirical relationships. In addition, the spectrum of ^{29}Si can provide a quantitative measure of relative site populations if the delay between successive radio frequency pulses is long enough to allow all relevant nuclei to fully equilibrate. The disadvantages of ^{29}Si are its very long spin-lattice relaxation time and its low natural abundance which leads to low sensitivity and long times for data acquisition.

High resolution ^{29}Si NMR has been extensively used for structural studies of the various silicate anions in solution[34-44]. These studies have established the identities of a whole series of silicate anions of different structure, due to polycondensation of the silicates. It was found that in silicate solutions the full range of ^{29}Si chemical shifts is over 500 ppm referred to tetramethylsilane (TMS), but the typical range of the isotropic chemical shift of ^{29}Si is from -60 to -120 ppm from TMS and is split up into well separated intervals corresponding to silicon atoms in monosilicates, SiO_4^{4-} groups, the tetrahedral Si without other tetrahedral Si neighbor, (denoted by Q^0), disilicates and chain end groups (Q^1), the tetrahedral Si with one neighboring tetrahedral Si by an oxygen bridge, middle groups in chain (Q^2), Si with two neighboring tetrahedral Si, chain branching site and sheet groups (Q^3), Si with three neighboring Si, and fully cross-linked framework sites (Q^4), all four corner O atoms are shared by other four tetrahedral Si. All silicate anions can be described using combinations of Q^n units, where the superscript refers to the number of silicon atoms linked,via oxygen bridges, to the central silicon.

Before the early 1970s, conventional NMR was used in studies of solid silicates. Due to the dipolar interactions between nuclear spins and the orientational anisotropy of the ^{29}Si chemical shielding, standard techniques led to relatively broad NMR line widths and to completely overlapping lines. For example, the NMR line width of $Na_2Si_2O_5$ measured in the solid is 208 ppm[45]. In 1956 Holzman et al.[46] were able to measure chemical shifts for silica (-113 ppm from

TMS), cristobalite (-113 ppm), quartz (109 ppm) and several multicomponent glasses (-93 ppm). In 1972 Gibby et al.[47] determined principal elements of the ^{29}Si chemical shielding tensor for a number of organosilicon compounds at -186°C using cross-polarization. But the broad line width has made conventional ^{29}Si NMR impractical as a general method for structure studies of solid silicates and aluminosilicates.

Lippmaa et al. first observed the existence of distinct ^{29}Si chemical shift ranges for different types of silicate structural units in crystalline materials. In 1978 they used magic angle spinning (MAS) combined with cross-polarization to obtain spectra of organosilicon compounds.[48] In 1980 they carried out a systematic study of numerous silicates composed of different types of Q^n units and aluminosilicates.[49] They found that the dominant feature determining the chemical shift of silicon in silicates is the degree of anion condensation, which leads to the formation of distinct and analytically significant chemical shift ranges according to the number of neighboring silicon-oxygen tetrahedra. Isotropic values of ^{29}Si chemical shifts in solids and solutions are generally the same and depend primarily on the degree of condensation of the silicon-oxygen tetrahedra. Increasing condensation from the single to double tetrahedra, to chains and cyclic, layered structures, and finally to three dimensional frameworks leads to increasing diamagnetic shielding of the ^{29}Si nucleus from about -65 to -70 ppm in monosilicates with about 10 ppm steps for each next type of condensation, and SiO_2 polymorphs resonate above -100 ppm from TMS. There are well-separated

and analytically useful ranges for each type of Q^n unit. The isotropic chemical shift ranges of ^{29}Si are -60 to -82 ppm for isolated silicate (SiO_4^{4-}) tetrahedra (Q^0), -68 to -83 ppm for pairs and chain end groups (Q^1), -73 to -94 ppm for rings and chains (Q^2), -91 to -98 ppm for chain branching sites and sheet (Q^3), and -105 to -120 for three dimensional framework (Q^4) silicates.[50]

The "Q notation" are used only for silicates. In framework silicates the neighbor tetrahedra of each Si are always four Si tetrahedra, denoted by $Si(OSi)_4$. In framework aluminosilicates some Si tetrahedra, SiO_4^{-4}, are substituted by Al tetrahedra, AlO_4^{-5}. Therefore, there are five possible species described by $Si[(OAl)_n, (OSi)_{4-n}]$ or simply $Si(OAl)_n$, where n=0,1,2,3 and 4. The symbol $Si(OAl)_n$ expresses that the Si atom is linked, via oxygens, to n aluminum and (4-n) silicon neighbors. Lippmaa et al.[49] also found that when one or more Si atoms in a framework are replaced by Al atoms, a significant paramagnetic shift results, i.e., the ^{29}Si chemical shift moves down-field. In general the substitution $Si(OAl)_{n-1} \rightarrow Si(OAl)n$ brings about a down-field shift of about 5-6 ppm. The isotropic ^{29}Si chemical shift ranges are -80 to -90 ppm for $Si(OAl)_4$, -85 to -94 ppm for $Si(OAl)_3$, 90 to -98 ppm for $Si(OAl)_2$, -96 to -107 ppm for $Si(OAl)_1$, and -106 to 120 ppm for $Si(OAl)_0$. The spectra of aluminosilicates were in good agreement with known crystal structures.[49,51] In 1984 it was observed that some other structural factors, such as electrostatic bond strengths of the cations, distortion of the bond angles in the silicon-oxygen tetrahedra,and changes in Si-O-Si bond angles, cause significant changes of the chemical shift of Si in silicates, thus lead to

overlapping of the ranges caused by differences in anion condensation[50].

^{29}Si chemical shifts are also capable of distinguishing crystallographically as well as chemically distinct silicate groups in polycrystalline and noncrystalline materials. Since the pioneering studies by Lippmaa, spectra of ^{29}Si in many silicates have been measured by various workers. Some of these results can be explained satisfactorily on the basis of previous identifications. Others cannot. The reason for this is that some silicates contain two or more kinds of crystallographically nonequivalent tetrahedral sites, each corresponding to a distinct value of the ^{29}Si chemical shift. When the chemical shift of a kind of site with silicons surrounded by n aluminum atoms is very close to that of another kind of site with silicons surrounded by n±1 aluminum atoms, the two spectral lines overlap and cannot be assigned simply.

The ^{29}Si MAS NMR is quantitatively reliable and the Si/Al ratio can be determined from the relative areas of peaks in the ^{29}Si NMR spectrum without resorting to a standard. The peak intensities correspond quantitatively to different $Si(OAl)_n$ species. The use of solid-state ^{29}Si NMR in the analysis of aluminosilicates is based on the observation by Lippmaa et al.[49] chat the ^{29}Si chemical shifts of aluminosilicates depend mainly on the number of Al atoms in the second coordination sphere of Si atoms. The five possible peaks were separated by approximately 5 ppm. It follows that when the peaks are correctly assigned in terms of $Si(OAl)_n$ units, there is no Al-O-Al linkage (Loewenstein rule), and the recycle time between each pulse is

long enough to allowed the thermal equilibrium of sample magnetization, the Si/Al ratio in the sample may be determined from the relative populations of the five possible peaks in ^{29}Si spectrum according to the following formula:[52-55]

$$(Si/Al) = \frac{\sum_{n=0}^{4} I_{Si(OAl)n}}{\sum_{n=0}^{4} \frac{n}{4} I_{Si(OAl)n}}$$

where $I_{Si(OAl)n}$ is the intensity of the $Si(OAl)_n$ peak. This equation is structure independent and can serve as a test for the correctness of peak assignments and the absence of Al-O-Al linkages. Although single-crystal X-ray diffraction measurements[56,57] on zeolite A (with Si/Al=1.00) led to the conclusion that the (cubic) space group of this zeolite is Fm3c, and that the Si and Al atoms alternate throughout the framework, and the presence of the single ^{29}Si resonance in the spectrum of zeolite A proves the existence of Si, Al ordering, Lippmaa et al.[51] claimed that in zeolite A each Si atom in the structure is linked to three Al atoms and one Si atom and each Al is linked to three Si and one Al due to its unusual chemical shift which is -89.2±1 ppm from TMS and was assigned to $Si(OAl)_3$ by Lippmaa et al. The controversy was resolved by Thomas et al.[53] and Melchior et al.[58] who examined the spectra of zeolite ZK-4. The ^{29}Si MAS NMR spectrum of ZK-4 contains several peaks and good agreement between $(Si/Al)_{nmr}$ and $(Si/Al)_{xre}$ ratios can be obtained only when the peak at -89.0±1 ppm is assigned to $Si(OAl)_4$ rather than $Si(OAl)_3$. They suggested that the

unusually low chemical shift of -89.0 ppm in zeolite A is due to the presence of a unique structure unit: strained double four-membered rings with Si-O-Al angles of 129, 152, 152 and 177°. The presence of the nearly linear linkages modifies the bonding, which in turn affects the value of the chemical shift. It seems that in retrospect Lippmaa's assignments were incorrect, and that the Loewenstein rule which forbids Al-O-Al linkages is obeyed by all zeolites. It is also seems reasonable that the Al-O-Al linkage may be present as structural defects. The calculation of Si/Al ratio is complicated in systems possessing inequivalent sites.[59-61] For example, erionite has two inequivalent tetrahedral sites, so two resonance for each Si(OAl)n unit which are separated by 5.6 ppm. Thus each peak is formed by the overlap of Si(OAl)n + Si(OAl)n_{+1} sites. The mordenite has the similar situation, where the spectrum is made up of three overlapping ^{29}Si peaks.

Melchior et al.[62] pointed out that without the restrictions of aluminum avoidance, e.g., the distribution of Si and Al in the framework were purely random, the average number of Al neighbors per Si atom would be equal to the average overall population: $\langle k\rangle=4/(1+R)$ where R=Si/Al. If however, with the aluminum avoidance constraint, Al-O-Al linkages were forbidden, the average number of Al neighbors would be $\langle k\rangle=4/R$. Murdoch et al.[63] and Klinowski et al.[55] further indicated that the value of $\langle k\rangle$ governs the location of the ^{29}Si peak maximum. Without the restriction of aluminum avoidance, the variance in the number of aluminum neighbors is given by:

$$\sigma^2 = \langle k^2\rangle - \langle k\rangle^2 = 4R/(1+R)^2.$$

The variance is a maximum ($\sigma^2 = 1$) when R = 1, and decreases with increasing R. With the restriction of aluminum avoidance, σ^2 is given by:

$$\sigma^2 = \langle k^2\rangle - \langle k\rangle^2 = 4(R-1)/R^2.$$

In this case the variance is zero (no disorder) for R = 1, achieves its maximum value of 1.00 for R = 2, and falls to 0.89 for R = 3. The variation σ^2 contributes to the NMR line width of ^{29}Si in glasses. As a result, it can be determined from the variation of width of different peaks that whether the Loewenstein's aluminum avoidance principle is obeyed or not, although it is not necessary for glasses to obey Loewenstein's rule. Murdoch found that the line widths as a function of the Si/Al suggest that the Loewenstein rule is largely obeyed.

Ohashi and Finger[64] observed the ^{29}Si MAS NMR spectra of enstatite ($MgSiO_3$, a pyroxene with single chains of Q^2 tetrahedra) and enstatite glass. The full width at half maximum of enstatite is 0.8 ppm but that of enstatite glass is 22.7 ppm. The width of the glass peak is due in part to variations in Si-O-Si bond angles and Si-O bond lengths, these being a natural consequence of the lack of long range order. In addition, there is the possibility of variation in the number of nonbridging oxygens per silicate tetrahedron. The $MgSiO_3$ glass peak actually encompasses the entire chemical shift range from Q^0 to Q^4 units. Dupree and Pettifer have presented a more detailed

analysis of the Si-O-Si bond angle distribution associated with a Si MAS NMR spectrum of vitreous silica. Their peak maximum appears to lie at -109 ppm, corresponding to an average angle of 145.5°.

There has been little work done on spin-lattice relaxation times of ^{29}Si in aluminosilicates. It was generally assumed that ^{29}Si spin-lattice relaxation times of aluminosilicates is controlled by spin diffusion from paramagnetic centers. This has been observed to be true for ^{29}Si in offretite and in Na-Y zeolite.[65] Farlee et al.[66,67] measured T_1's in various hydrated zeolites and found that, for each sample, T_1's of a silicon atom in a Si(OAl)n unit varies little with n, and is also insensitive to a change in the Si/Al ratio. This indicates that ^{29}Si relaxation is not affected by the presence of ^{27}Al and also explains why short recycle times which were much shorter than $5T_1$ and used by most workers still give quantitatively reliable spectra. Sometimes this is not the situation. In the present work, the T_1's of Si atoms corresponding to different Si(OAl)n units in two aluminosilicate glasses were estimated, the T_1's in one sample are identical but the T_1's in ZERODUR do vary significantly with n.

^{27}Al NMR Studies of Aluminosilicates

In addition to ^{29}Si, ^{27}Al is another favorable nucleus for NMR investigations of aluminosilicates. In contradistinction to ^{29}Si, ^{27}Al has spin I=5/2, greater than 1/2, and possesses a quadrupole moment. Therefore the quadrupole interaction between the nuclear quadrupole

moment and the electric field gradient must be considered. With quadrupolar nuclei of noninteger spin, the central ($1/2 \longleftrightarrow -1/2$) transition, the only one which is normally observed, is independent of the quadrupolar interaction to first-order in perturbation theory. It is, however, affected to second-order and at moderate field strengths these second-order quadrupolar effects dominate the spectra, obscuring chemical shift effects which are related to short-range structure. The characteristic width for a quadrupole nucleus is

$$\Delta\omega_{1/2} = \frac{\omega_Q^2[I(I+1)-3/4]}{12\omega_L}.$$

For $I=5/2$, $\Delta\omega_{1/2} = 2\omega_Q^2/3\omega_L$ where ω_L is the Larmor frequency and ω_Q is the quadrupole frequency.[68] The magnitude of the second order quadrupolar interaction is inversely proportional to the magnetic field strength. Thus the higher the magnetic field strengths, the narrower will be the width of the central transition. Under MAS, the influence of the dipolar interaction, the anisotropy of the chemical shift and the quadrupole interaction in first-order on the line width vanish, but it is not possible to average the second-order quadrupolar line-broadening in ^{27}Al NMR spectra to zero and it can only be diminished and modified. The variable angle sample spinning (VASS) technique[69,70] can provide sharper lines of quadrupolar nuclei in some samples but it cannot average other line-broadening interactions to zero and its use is limited. Also unlike ^{29}Si, ^{27}Al has a 100% natural abundance and its spin-lattice relaxation time is very short.

This makes ^{27}Al MAS NMR very sensitive; even traces of aluminum are detectable. In addition, the linewidth of the ^{27}Al resonance signal is sensitive to the symmetry of the nuclear environment. If the ^{27}Al nuclei is at the center of an environment of cubic symmetry, the electric field gradient is zero and the second-order quadrupole interaction is zero too, although in practice there are always broadenings associated with crystal imperfections.

The spectra of alkaline aluminate compounds have been extensively studied. Akitt et al.[71-79] found that in aluminate anion solution four-coordinated aluminum (with respect to oxygen) has a chemical shift range of 60-80 ppm downfield from the six-coordinated Al in $Al(H_2O)_6^{3+}$. Muller et al.[80] resorted to tetramathylammonium aluminosilicates to measure ^{27}Al chemical shifts in aluminosilicate solutions. They also found that dimeric aluminate anions are found only in very concentrated solutions and even then in very small quantities, and suggested that the Loewenstein rule is obeyed in aluminate and aluminosilicate anions.

In 1981 Muller et al.[81] studied ^{27}Al NMR spectra of polycrystalline aluminates. High resonance frequencies of 70.4 MHz were used to reduce the quadrupole interaction in second order. Similar to that in aqueous solutions, the isotropic ^{27}Al chemical shifts depend mainly on the coordination of aluminum with respect to oxygen. The chemical shifts of tetrahedrally coordinated ^{27}Al are 55-80 ppm downfield from $Al(H_2O)_6^{3+}$, and those of octahedrally coordinated Al are 0-22 ppm. The presence of a range of ^{27}Al chemical shifts, both for four- and six-coordinated aluminum indicates that the chemical shift values are influenced not only by the coordination of the Al, but

also by other effects such as the composition of the second coordination sphere and the nature of the cation. The results shows that solid state high resolution ^{27}Al NMR is a useful tool for determination of Al-O coordination. In addition to the four- and six-coordinated aluminum, in 1985 Cruickshank et al.[82] recorded the ^{27}Al MAS NMR spectrum of a new barium aluminate glycolate[83] in which the aluminum was penta-coordinated by oxygen alone. The spectrum of the new aluminate shows a single peak at 35.3 ppm downfield from the peak of $Al(H_2O)_6^{3+}$, suggesting that five-fold coordination should be identified by observing NMR between the octahedral (about 0 ppm) and tetrahedral (about 70 ppm) position. Gilson et al.[84] studied ^{27}Al MAS NMR of various aluminosilicates and found that upon thermal or hydrothermal treatment a line at ~30 ppm, corresponding to penta-coordinated Al, appears for all these aluminosilicates.

The resolution of ^{27}Al MAS NMR spectrum was substantially improved by the combination of the technique of magic angle spinning and increasing the magnetic field. The improvement, not only involves the reduction of second-order quadrupolar interaction, also the increased intensity and symmetry. Freude and Behrens[85] studied the ^{27}Al MAS NMR of zeolites and found that when the sample spins at frequency greater than ω_Q^2/ω_L the peak width is reduced to 1/3 of its original value. Fyfe et al.[86] studied the ^{29}Al spectra of dealuminated zeolite Y using silicon tetrachloride. They found that an additional ^{27}Al signal appears at 0.0 ± 2 ppm, due to residual six-coordinated Al and there is a large change in the chemical shift of tetrahedrally coordinated Al, from 61.3 ppm in the parent material to 54.8 ppm in the

dealuminated product. The later effect indicated that the chemical shift is related to the neighbering AlO_4^{5-} tetrahedron. The first order tetrahedral neighbors are always four Si due to the Loewenstein rule, so the actual magnitude of the shift must be governed by geometric factors such as T-O-T bond angles and by the composition of tetrahedral coordination shells beyond the first order and the effect is quite long range in nature.

^{27}Al MAS NMR normally detects a single signal, attributable to $Al(OSi)_4$. But when using very high magnetic fields, ^{27}Al MAS NMR spectroscopy is capable of resolving crystallographically nonequivalent, tetrahedrally-bonded Al atoms. Klinowski et al.[87] found that there two separated lines in ^{27}Al MAS NMR spectrum of zeolite omega at 130.32 MHz due to the two nonequivalent sites, in agreement with the structure of this zeolite. But these two peaks cannot be separated at 52.11 MHz, which implies that the second order quadrupolar effects are relatively large. Fyfe et al.[88] found that the peak at 55.6 ppm from that of $Al(H_2O)_6^{3+}$ in ^{27}Al MAS NMR spectrum of silicalite is characteristic of tetrahedral coordination. This peak has a maximum at 54.5 ppm and a shoulder at 56.7 ppm indicating the presence of crystallographically nonequivalent sites for tetrahedral Al. Therefore at least two distinct types of tetrahedral framework sites are occupied by the aluminum atoms.

Theoretical Background and Consideration

NMR spectral lines from solid specimens are very much broader than those from liquids. This substantial difference arises from the static anisotropic interactions which are averaged in the liquid state and effectively removed from the spectrum by the rapid and isotropic thermal motion of molecules. By contrast, generally there is little internal motion in the solid state. For a deep understanding of high resolution NMR spectra of solid powder samples, it is necessary to examine the various magnetic interactions in an ensemble of nuclear magnetic moments.

In general the anisotropic nuclear interactions which are of interest in solid state NMR spectroscopy of aluminosilicates are the following:[89]

(1) The dipole-dipole interactions:

The magnetic dipole interaction are the interaction between nuclear moments $\gamma_i h I^i$ and $\gamma_j h I^j$. The interaction Hamiltonian is

$$h\mathcal{H}_D = \frac{\gamma_i \gamma_j h^2}{r_{ij}^3} \left[I^i \cdot I^j - 3 \frac{(I^i \cdot r_{ij})(I^j \cdot r_{ij})}{r_{ij}^2} \right]$$

where γ_i, γ_j are the nuclear gyromagnetic ratios, r_{ij} is the internuclear vector.

To calculate the lineshape in solids, first order perturbation theory is applied. Because the amplitude of internal thermal motion is

low and the probability of induced transitions is small, only part of H_D, the secular dipolar Hamiltonian H_D^{sec}, is involved in these evaluations. Nonsecular terms in the Hamiltonian joining states of different energy are usually negligible in the calculation of energy levels.

For the homonuclear case ($\gamma_i=\gamma_j=\gamma$), the secular dipolar Hamiltonian $H_{D,II}^{sec}$ is given by

$$H_{D,II}^{sec} = \Sigma \frac{\gamma^2 h\mu_o}{4\pi r_{ij}^3} \cdot -(\frac{1}{2} - 3\cos^2\theta_{ij})(3I_z^i I_z^j - I^i \cdot I^j)$$

For the heteronuclear case ($\gamma_i=\gamma_I \neq \gamma_j=\gamma_S$), the secular Hamiltonian takes the form

$$H_{D,IS}^{sec} = \Sigma \frac{\gamma_I \gamma_S h\mu_o}{4\pi r_{IS}^3}(1 - 3\cos^2\theta_{ij}) I_z S_z$$

where θ_{ij} is the angle between r_{ij} and the Zeeman field B_o, which is directed along the z-axis in the laboratory frame of reference. The dipole Hamiltonian indicates that:

(a) The thermal motion of molecules in fluids averages the dipole interaction between spin 1/2 systems to zero due to the isotropic average $\overline{\cos^2\theta}$ which is 1/3.

(b) Dipole-dipole interactions are often dominant in solid powder samples, producing dipolar powder patterns that are so broad (several KHz) that they obscure any high-resolution information

in the spectrum. But the dipole interaction is proportional to the inverse of the cube of the internuclear distance. The strong dependence of the dipole interaction on internuclear distance implies that the dipole interaction is important only for nuclei in close proximity. The natural abundance of ^{29}Si is 4.7%. As a result the average value of distance between 'diluted' ^{29}Si nuclei is sufficiently large that the homonuclear dipolar interaction is averaged to zero by MAS (vide infra). In aluminosilicate glasses the same applies to the ^{27}Al-^{27}Al interaction because of the Loewenstein rule which forbids aluminate tetrahedra as neighbors of each other in the framework. The heteronuclear dipolar interaction is similarly negligible under MAS in aluminum silicates because the aluminum-silicon distance is about 3.0 Å and the dipolar splitting at ^{29}Si due to ^{27}Al is $\delta=\gamma_1\gamma_2 h/(2\pi)^2 r^3=6303/r^3=233$ Hz.

(c) The first try to emulate nature by imposing a motion on the nuclei was done by rapidly spinning the solid specimen in 1959 by Andrew and Wynn[3] and Lowe[90]. They indicated that for polycrystalline and amorphous materials, if the solid specimen rotates rapidly and uniformly about an axis inclined to magnetic field at angle β, the time-average value of the angle between all internuclear vectors and the magnetic field $\theta_{ij}=\beta$. The spectrum is reduced in width by the scale factor:

$$F(\beta) = |(1/2)(3\cos^2\beta - 1)|$$

This is most effective when β is the 'magic angle', 54.74°, called magic angle spinning, so that $3\cos^2\beta - 1 = 0$ and the value of $F(\beta)$ is zero. This result is true for both homo- or hetero-nuclear dipolar interactions for weak quadrupolar nuclei like ^{27}Al. Under rapid sample spinning at the magic angle, all dipolar interactions between spin 1/2 nuclei are averaged to zero and are removed, but MAS will not completely remove the dipolar interaction between a spin 1/2 and a nonspin 1/2 nucleus.

(2) The chemical shift anisotropy

The chemical shift is due to the shielding of external magnetic field $\mathbf{B}_0$, at a given nuclear magnetic moment by the surrounding electrons. This internal magnetic field at the nucleus opposes the $\mathbf{B}_0$ and has a strength proportional to $\mathbf{B}_0$. It is also spatially anisotropic, known as 'chemical shift anisotropy'. The chemical shift interaction is described by the Hamiltonian $\mathbf{H}_{CS}$

$$\mathbf{H}_{CS} = h\gamma \mathbf{I}\cdot\boldsymbol{\sigma}\cdot\mathbf{B}_0$$

where σ is the chemical shift tensor which is a second rank tensor.

The influence of chemical shift can be calculated by first-order perturbation theory because of its small contribution to the Zeeman energy. Also, only the secular part of Hamiltonian, H_{CS}^{sec}, is considered

$$H_{cs}^{sec} = \gamma B_o I_z \sigma_{zz}$$

where $$\sigma_{zz} = \sigma + -\delta_{cs}[3\cos^2\theta - 1 + \eta_{cs}\sin^2\theta\cos 2\Phi]$$

where σ is the isotropic shielding, δ_{cs} the anisotropy parameter and η the asymmetry parameter.

Unlike the dipole interaction tensor which is a traceless, axially-symmetric second rank tensor, σ is not traceless. In large magnetic fields, σ is symmetric and can be described by three principal values, σ_{11}, σ_{22}, σ_{33}, and the angles which define the orientation of the principal axis. It has been shown[3,91] that when the sample is spun at an angle β to the magnetic field B_o the time-averaged value of the tensor component along B_o is

$$\overline{\sigma_{zz}} = \frac{3}{2}\sigma\sin^2\beta + \frac{1}{2}(3\cos^2\beta - 1)\sum_j^3 \sigma_{jj}\cos^2\chi_j$$

where $\sigma=(1/3)(\sigma_{11}+\sigma_{22}+\sigma_{33})$ and χ_j is the angle between the spinning axis and each of the three principal axes. Consequently when $\beta=54.74°$, $\cos^2\beta=1/3$, $\sin^2\beta=2/3$, σ_{zz} reduces to the scalar isotropic value σ, and the shift anisotropy is removed from the NMR spectrum for every nucleus in the specimen whatever the degree of anisotropy or asymmetry of its shift tensor and whatever the orientation of its principal axes.

(3) The nuclear electric quadrupole interaction

Nuclei with spin $I>1/2$ possess a quadrupole moment eQ and may interact with electric field gradients (EFG) present in the solid. The EFG is described by the traceless symmetric tensor[92]

$$V_{ij} = \frac{\partial^2 V}{\partial x_i \partial x_j}$$

where V is the electric potential and x_i and x_j are Cartesian coordinates. In the principal axis system of V_{ij}, in which the tensor is diagonal, the quadrupolar Hamiltonian for a single spin is

$$H_Q = \frac{e^2qQ}{4I(2I-1)}[3I_z^2-I^2+\eta(I_x^2-I_y^2)].$$

In the case of ^{27}Al in aluminosilicate glasses the magnitude of H_Q is smaller than H_Z. Then H_Q can be treated as a perturbation on the Zeeman levels. The various energy levels $E_m^{(0)}$, $E_m^{(1)}$, and $E_m^{(2)}$ (superscripts denote perturbation order) of the above equation are obtained using perturbation theory. The $E_m^{(0)}$ part includes the Zeeman energy. Instead of a single resonance frequency

$$\omega_L=(E_{m-1}^{(0)}-E_m^{(0)})/h,$$

as in the case of spin 1/2, there are several resonance frequencies with contributions to second order in perturbation;

$$\omega_m = \omega_L + \omega_m^{(1)} + \omega_m^{(2)},$$

For ^{27}Al which has a nonintegral spin, 5/2, only the central $-1/2 \leftrightarrow 1/2$ transition is generally observed in single pulse experiments, as the other transitions are spread over too wide a frequency rage.

If the electric field gradient is axially symmetric ($\eta_Q=0$), the expressions for the first- and second-order frequency shifts, are

$$\omega_m^{(1)} = -(1/2)\omega_Q(m-1/2)(3\cos^2\theta - 1),$$

and

$$\omega_{1/2}^{(2)} = -(\omega_Q^2/16\omega_L)(a-3/4)(1-\cos^2\theta)(9\cos^2\theta - 1).$$

where

$$\omega_Q = 3e^2qQ/2hI(2I-1),$$

$$\omega_L = \gamma B_0(1-\sigma)/2\pi,$$

and $$a = I(I-1)$$

For the case of ^{27}Al which has I=5/2, the first order frequency shift vanishes for m=1/2, which means that for half-integer spin nuclei the quadrupole interaction contributes only in second and higher-order perturbation theory. The second-order shift is not scaled by $(3\cos^2\theta - 1)$. It is inversely proportional to the magnetic field (through ω_L). So a better way for studying ^{27}Al in aluminosilicate glasses is to observe the central transition of nuclei, use MAS to remove dipolar interactions and chemical shift anisotropy, and work at high fields to minimize second-order effects and to maximize the chemical shift. In practice, only $1/2 \longleftrightarrow -1/2$ transition is observed in solid samples, showing a characteristic powder pattern depending on the value of of the asymmetry parameter η. Magic angle spinning reduces but does not

eliminate the width of this powder pattern. A formula for the frequency of the -1/2⇔1/2 transition under fast magic angle spinning conditions has been derived by Kundla et al.[93] and Samoson et al.[94] and was rewritten by Kentgens et al.[95] as

$$\omega_{1/2,-1/2} = \omega_z - \frac{\omega_Q^2}{16\omega_z}\{I(I+1) - \frac{3}{4}\}\{A(\alpha)\cos^4\beta + B(\alpha)\cos^2\beta + C(\alpha)\}$$

where

$$\omega_z = -\gamma B_0(1 - \sigma_i)/2\pi$$

$$\omega_Q = 3e^2qQ/\{2I(I-1)h\}$$

$$A(\alpha) = (7/2) - (7/3)\eta\cos2\alpha + (7/18)\eta^2\cos^2 2\alpha$$

$$B(\alpha) = -3 + (2/9)\eta^2 + (8/3)\eta\cos2\alpha - (7/9)\eta^2\cos^2 2\alpha$$

$$C(\alpha) = (5/6) - (1/3)\eta\cos2\alpha + (7/18)\eta^2\cos^2 2\alpha$$

and α and β are the polar angles of the spinning axis with respect to the principal axis of the quadrupole tensor. Kundla et al. showed the numerically calculated powder pattern lineshapes of the central -1/2 ⇔ 1/2 transition of half-integer spins in the fast rotation limit by the above equation (see Figure 1).

EXPERIMENTAL

Consideration

Magic angle spinning (MAS) as a line narrowing technique is very useful in NMR studies of solid state due to the fact that spinning is a method of narrowing NMR lines broadened by the dipole-dipole interaction and the large anisotropic chemical shielding terms generally found in solid powder samples. Magic angle spinning rates in commercial spectrometers have typically not exceeded 5 KHz. This is usually sufficient to reduce the sidebands generated to an acceptable level. But ZERODUR glass has some characteristics that make quantitative measurements of its NMR spectrum difficult.

First, for measurements of ^{29}Si NMR, due to its low natural abundance (4.7%) and low NMR sensitivity (7.84×10^{-3} relative to ^{1}H), the signal-to-noise ratio (S/N) is poor. Improving S/N by increasing the number of data accumulations is limited by its long longitudinal relaxation times, T_1, which were estimated to be between 300 to 1000 seconds for different $Si(OAl)_n$ species. The long values of T_1 necessitate long delays ($5T_1$) between 90° pulses in a FT NMR experiment. An audio filter with 3 KHz bandwidth had been used to improve S/N. Although use of the narrow band filter increases S/N significantly, it caused a dead time of 230 μs after a pulse. As a

consequence, the relative intensity of the broad line in the NMR spectrum of ZERODUR was severely reduced due to its short T_2. One way to improve S/N is to increase the quantity of sample. The static NMR spectral width of Si in ZERODUR is about 80 ppm. Therefore a spinning speed of 3 KHz and a large rotor volume were needed to avoid problems of quantitation associated with spinning sidebands and to maximize S/N.

Second, the ^{27}Al atom with spin I=5/2 has the nuclear quadrupolar interaction which gives rise to a broadening of the central transition which was usually observed. This broadening cannot be totally removed by magic angle spinning. The NMR signal of tetrahedral Al is about 50 ppm down field from that of octahedral Al. If the spinning speed of the sample is not sufficiently high, the spinning sides bands will overlap with the central transition corresponding to Al atoms in Td and Oh sites. A minimum spinning speed of 7 KHz is needed to separate the side bands from the peaks corresponding to chemically shifted sites.

Amorphous Si also presents the problem of low sensitivity, long longitudinal relaxation times after annealing at 490^{o}C, and broad spectral width due to its structure disorder. It also requires a large sample volume, and a spinning speed faster than 4.5 KHz to separate the sidebands from the isotropic peak.

Probe Construction

In order to solve the above two problems, a new probe was needed for measuring NMR spectra of both ZERODUR and amorphous Si. The initial goals of designing the probe were as follows:

(1) large rotor volume (about 0.7 mm^3) for ^{29}Si measurements

(2) high spinning speed for ^{27}Al measurements

(3) easy and accurate magic angle adjustment

(4) variable, stable and reproducible spinning speed

(5) use of dry air as driving gas due to its low cost relative to helium.

All MAS systems depend on gas jets to provide the driving force and some type of air bearing to provide support and stability. Most of the spinning systems that have been reported in the literature are modifications of either the conical spinner pioneered by Beams[96,97] and implemented in MAS NMR experiments by Andrew and Wynn[3] or the cylinderical spinner introduced by Lowe[90]. Both types of spinners were reported to work satisfactorily. P. A. S. van Dijk et al. found that the orientation of the spinner rotation axis of conical types is influenced by slight imbalances of the rotor and depends on the rotation speed[98]. When a compressed gas jets from a straight tube, its maximum speed is the speed of sound. The ultimate rotation rate of a gas-driven rotor is governed by the linear velocity of its periphery. So the maximum velocity of the rotor periphery may not exceed the speed of sound. For example, a 9-mm-diameter rotor has a maximum theoretical

rotation rate of 11.7 KHz in dry air. When helium is used as driving gas, where the speed of sound is 2.7 times greater, the maximum theoretical rate would be 31.5 KHz. Usually the use of helium as driving gas can double the spinning speed of rotor driven by dry air. In practice it is possible to approach only some fraction of these maximum rotation rates.

Although the basic design of the spinner used in this study is similar to that developed by Wind et al.[99], several important modifications necessary for fast and stable spinning were introduced. Figures 2-5 show the design of the spinning system.

The rotor made from Torlon is cylinderical with eight flutes machined into its bottom surface. There is a tightly fitted cap made from KEL-F or Torlon on its top. The symmetry of both rotor and stator is critical for spinning at high speed. The tight fitting construction is more symmetrical than that of a threaded construction, and reduces the imbalance when the rotor is spinning. The Torlon rotor is strong enough to withstand the tensile stress caused by the mass of sample and the high spinning speed. There is no observable distortion of the rotor after spinning for periods as long as two weeks.

Outside the stator is a brass seat with two air inlets on its side, one for the driving air and the other for the air bearing. At the center of the seat's bottom there is an adjusting bolt which supports and keeps the rotor at the right location in driving air so that the highest spinning speed can be achieved. The location of rotor in driving air is critical for obtaining maximum spinning speeds. The supporting bolt must be adjusted very carefully. The heavy mass of the

brass seat reduced the vibration frequency caused by the spinning rotor.

The stator is made of KEL-F and fits into the seat tightly. The stator is similar to those built by Wind. An air bearing ring made from brass is tightly fitted into the center of the stator. On the stator, there are 24 bearing air holes, which are separated evenly in three planes perpendicular to the center line of the stator. These air holes go from the bearing air chamber through the air bearing ring towards the center line of the spinner. There are also four driving air holes on the stator, which are at 30° with respect to the line through both centers of stator and nozzle in the plane perpendicular to the center line of stator and also 9° with respect to the same plane, pointing towards the bottom of the rotor. Spinning of the rotor is effected by the dynamic action of propellant gas streaming from the four nozzles against the eight flutes on the bottom of rotor. Increasing the pressure of driving air increases the spinning speed but reduces the spinning stability. Increasing the pressure of the bearing air has an opposite effect. So the air pressures for the nozzles and for the bearing are regulated separately to obtain the fastest and most stable spinning. Both driving and bearing air chambers, which are formed and sealed to the outside by the press fit between stator and seat, were enlarged to 18 mm o.d. to minimize the unevenness of the air pressure in the chamber. Also the inlets were enlarged to 3 mm i.d. in order to minimize the pressure drop from the air source to the chamber. Both effects are important for increasing spinning speed and stability. Both driving and bearing air jets were tested using a variety of hole

sizes from 0.5 mm to 1.0 mm. No significant effect was found on increasing the highest spinning speed. The bigger the hole size, the lower the pressure used. Stators of various sizes may be inserted in the seat. Two different stators were used. One had an air bearing ring of 9 mm i.d. and the other an air bearing ring of 5 mm i.d. A 9 mm rotor with a 7.5 mm i.d. was used with the 9 mm stator for 29-Si NMR of ZERODUR and amorphous Si. The rotor filled with sample was able to spin at 6.0 KHz using an air drive. The rotor can accommodate 0.75 cc of powdered sample and the large quantity of sample improves the S/N. A 5 mm rotor with a 4 mm i.d. was used with the 5 mm stator for 27-Al NMR of ZERODUR. With the sample loaded, it was able to spin at 10 KHz, fast enough to separate the spinning side bands from the isotropic peaks. The most critical size of the spinner is the gap between the rotor and the air bearing ring. It was found that 0.15 mm (0.06 inch) is the best. There is no significant variation found in the spinning rate with the direction of the spinning axis (vertical, horizontal, upside down or "magic angle").

A problem arising from spinning at high speed is the lifetime of rotor. When the rotor is spinning, the adjusting bolt at the bottom center of the stator seat (see Figure 1) supports the rotor and keeps the rotor at the right location in the driving air. The contact between the high speed rotor and the static adjusting bolt severely wore the center of the rotor bottom. The result was that the rotor could not be kept at the right location in the driving air, and the rotor spinning was unstable. During a short period of about 2 minutes, the fluctuation of the spinning speed was found to be about ±250 Hz due

to the contact. During longer period of about 2-3 hours, the wear of the contact point varies the location of rotor in the driving air and causes a drop in spinning speed by 2 KHz. The average lifetime of the rotor was about only 3 hours.

To solve this problem, the design shown in Figure 1 was similar to that of Wind, but incorporated an air bearing at the bottom of rotor as well as on the sides as suggested by Marek Pruski in our group. The second bearing air, introduced through the center of the adjusting bolt had significant effect on rotor lifetime and spinning stability. When the rotor is spinning with the second bearing on, the pressure of which was regulated separately, a small gap can be seen between the rotor and adjusting bolt. After ten days continuously spinning at 4.5 KHz for 9 mm rotor and at 9 KHz for 5 mm rotor, the bottom of the two rotors showed no obvious wear. The second advantage of the second bearing air is that it stabilizes the spinning speed. When the 9 mm rotor was spun at 4 KHz, the fluctuation of spinning speed was only ±1 Hz during a period of 5 hours. Furthermore, the spinning speed was also increased by about 5-7 hundreds Hz for both 5 mm and 9 mm spinner. The spinning rate can be varied smoothly and easily from about 250 Hz to the highest speed, 6 KHz for 9 mm spinner or 10 KHz for 5 mm spinner, by varying the pressures of both diving air and bearing air.

The spinning speed of the rotor was measured by an optical device. The flat top of the rotor cap was painted half white and half black as a reflector. A strong light is piped in through a bundle of optical fibres and illuminated the top of rotor cap. The reflected light varied following the spinning rotor and was picked up by a light

sensitive diode, the resistance of which varied following the reflected light and causes a voltage variation across the diode (see Figure 6). The voltage signal was then amplified using the circuit shown in Figure 6 and detected by an oscilloscope or a digital frequency meter.

The magic angle was adjusted by inclination of the seat of the spinning system about an axis perpendicular to the centerline of the stator. The mechanism is shown in Figure 7. The magic angle adjustment is capable of a precision of better than three hundredths of a degree. It has a bolt with two threads of different pitchs on its two ends. The bolt is arranged such that when it is turned the thread at one end increases the angle and on the other end simultaneously decreases the angle. Because of the different pitchs of the two threads the two angle variations are different. The resultant total angle variation is the difference of the two. In this probe two pitches of 36 per inch and 40 per inch are used. Each turn of the bolt causes a movement of 25.4/36 - 25.4/40 = 0.0706 mm. The distance from the rotation axis of the stator to the adjusting point is 38 mm. At the magic angle which is 54.74°, the 0.07 mm movement of the adjusting point corresponds to 0.086° angle variation. The adjustment of the magic angle was made using the NMR of ^{79}Br in KBr. An example of the rotational echos obtained on this sample is shown in Figure 8.

The coil form was threaded on the outside chimney of the stator (12 turns, 16 turns per inch for both 5 mm and 9 mm stator). The probe circuit is simple and shown in Figure 9. Tuning and matching capacitors were located physically near the coil. The electrical components were encased in a probe head that was 2 inches in diameter

and 3 inches in height. Probe tuning and magic angle adjustment is accomplished in place by tuning the vertically arranged variable capacitors and magic angle adjustment with long adjusting rods from the bottom of the magnet.

Experimental

All NMR experiments on ^{29}Si and ^{27}Al were performed in a home-built pulsed NMR spectrometer. A detailed description of the spectrometer can be found elsewhere[100] The probe described above was used for all measurements.

The spectrometer operated at 43.72 MHz for ^{29}Si. The 9 mm rotor, a dwell of 10 microseconds, a 20 KHz low pass filter, and zero resonance offset were used. The Q value of the probe is about 100, and the probe and filter have a combined ringdown time of 30 μsec. This ringdown time causes a relative error of less than 0.5% in intensities of broad and narrow lines in the spectra due to their different T_2. In order to estimate the T_1s of different $Si(OAl)_n$ species and to obtain correct spectra, three sets of data were taken. one was taken using a 90° pulse and 200 seconds recycle time. The second set of data was taken using a 90° pulse and 700 seconds recycle time. These two sets of data were used to estimate the T_1s of each $Si(OAl)_n$ species and to determine the experimental parameters used in taking the third set of data. The third set of data was taken using a 4° pulse and a 50 seconds recycle

time to obtain an undistored ^{29}Si spectrum of the two glass samples (see below). The rotation speeds of samples were 5 - 5.2 KHz.

The ^{27}Al spectra of the two glass samples were taken at 57.34 and 76.74 MHz, respectively, while sample was spinning at 8 KHZ. The 5 mm rotor, a dwell of 2 microseconds, a 100 KHz low pass filter, zero resonance offset, 30° pules, and 0.8 seconds recycle time were used in experiments.

All data were accumulated with spin temperature inversion of the excitation pulses and change in sign of alternate sets of accumulated data in order to minimize artifacts associated with pulse breakthrough, DC offset, and 60 Hz noise. After a linear tapering of the later part of the transient where basically only noise is evident, an 4K fast Fourier transform was performed.

The glass under investigation was an aluminosilicate material produced by Schott Optical Glass, Inc., under the trademark ZERODUR, with approximate composition by weight of 61% SiO_2, 23% Al_2O_3, 6% P_2O_5, 4% Li_2O, 2% TiO_2, 1.4% ZnO, and 1% or less of other oxides. Chemical analysis by Galbraith Laboratories, Inc. yielded a silicon to aluminum ratio of 2.0. ZERODUR has very low thermal expansion, and was used in optical equipment especially in large astronomical telescopes and laser instruments.

Another glass sample is used as a comparison, called glass 2. It has a similar structure as ZERODUR but different composition. The chemical analysis yields a Si/Al of 2.6.

Both sample were powdered before taking the data.

RESULTS AND DISCUSSION

When a sample is immersed in a strong magnetic field, the sample becomes magnetized and the magnetization of the sample increases exponentially with time according to the relation

$$M_0 = M_{eq} [1 - \exp(-t/T_1)].$$

Theoretically, after an infinite time, an equilibrium value of magnetization, M_{eq}, will be reached, but practically after $5T_1$, where the T_1 is the spin-lattice relaxation time, the sample magnetization will be more than 99.5 per cent of M_{eq} value. The M_{eq} is proportional to the population of atoms under investigation. There are 5 possible species, Si(OAl)n where n=0,1,2,3,4, in aluminosilicate glasses. When the T_1's of all ^{29}Si of the 5 units are identical, a recycle time shorter than $5T_1$ can still give a qualitatively reliable spectrum. When T_1's of ^{29}Si in different Si(OAl)n units are different, if the recycle time is shorter than $5T_1$, the magnetization of species with short T_1 is closer to its equilibrium magnetization value than that of species with long T_1. In consequence the relative intensities of different peaks in ^{29}Si NMR will be distorted. In this situation the recycle time in experiments is usually kept longer than five times of the longest T_1 to allow full equilibrium.

The T_1's of ^{29}Si in ZERODUR are relatively long (~ 1000 sec). To estimate the values of T_1 for ZERODUR two sets of data were taken using 90° pulse, one with recycle time of 200 seconds and another 700 seconds. The two Fourier transformed spectra are shown in Figure 10 and 11. Four peaks can be seen obviously at -113.7 ppm, -107.7 ppm, 101.6 ppm and -95.6 ppm referenced to tetramethylsilane (TMS). It also can be seen that the relative intensities of the two peaks at -113.7 ppm and -95.6 ppm decrease when recycle time is shorter. This indicates that the spin-lattice relaxation time T_1 of ^{29}Si in ZERODUR varies with the number of aluminum neighbors and the presence of ^{27}Al around a ^{29}Si may effects its relaxation.

Due to the lack of resolution of the ^{29}Si MAS NMR spectra of ZERODUR, a nonlinear least-squares curve fitting program was used to deconvolute the spectrum to a superposition of peaks and obtain the Si(OAl)n distributions. When approximate values are given for the peak positions, peak heights and full widths at half-maximum (FWHM) of the resonances, the program automatically varies these values and minimizes the deviation of the simulating curve from the experiment spectrum. In using this program, only obvious peaks and steps can be fitted. It was found that use of Lorentzian or mixtures of Lorentzian and Gaussian line shapes resulted in poorer fits than those of pure Gaussians. It was also found that the spectra of ZERODUR cannot be fitted well by only four peaks. When four peaks were used to fit the spectra the smallest peak at 113 ppm always moved to about 102 ppm and became a high and broad peak and the small shoulder at 113 ppm was left alone. So the two spectra of ZERODUR were fitted to a sum of five Gaussian

peaks. The fitted results are stable and shown in Figures 10, 11, and given in Tables 1 and 2. According to the chemical shift range of Si(OAl)n, the four peaks at -113 ppm, -108 ppm, -102 ppm and -96ppm were assigned to $Si(OAl)_0$, $Si(OAl)_1$, $Si(OAl)_2$ and $Si(OAl)_3$, respectively. No peak was assigned to $Si(OAl)_4$

The magnetization of sample in an external magnetic field is along the field direction which is defined as the z direction. In the rotating frame after a pulse of flip angle θ was applied along the x direction, the y component of the sample magnetization is $M_0\sin(\theta)$, and the z component is $M_0\cos(\theta)$, where the M_0 is the magnetization of the sample just before the applying of the pulse. The integrated peak intensity, H, of the NMR spectrum is proportional to the y component. When $\theta = 90°$, the peak integrated intensity proportional to M_0 and the z component of sample magnetization is zero. Then the z component of magnetization at time t after a 90° pulse is

$$M = M_{eq} [1 - \exp(-t/T_1)]$$

In a NMR experiment successive pulses are applied. With t the recycle time,

$$M_0 = M_{eq} [1 - \exp(-t/T_1)]$$

and

$$H_0 = H_{eq} [1 - \exp(-t/T_1)]$$

where H_0 is the peak height of the Fourier transformed spectrum which is proportional to M_0. When data were taken with a 90° pulse and two different recycle times, two different H_0s can be obtained from the spectra,

$$H_{01} = Heq\ [1 - \exp(-t_1/T_1)]$$

and

$$H_{02} = Heq\ [1 - \exp(-t_2/T_1)]$$

T_1 can then be estimated using

$$H_{01}/H_{02} - [1-\exp(-t_1/T_1)]/[1-\exp(-t_2/T_1)] = 0$$

From the data in Table 1 and 2 the T_1 of each Si(OAl)n were obtained by a computer program. The resultant T_1's of the five peaks are 1014 seconds for $Si(OAl)_0$, 677 seconds for $Si(OAl)_1$, 458 seconds for $Si(OAl)_2$, 304 seconds for the broad peak and 618 seconds for the $Si(OAl)_3$, respectively. It is noted that the T_1 varies significantly from about 300 seconds to 1000 seconds for the species characterized by the chemically shifted peaks in the NMR spectrum.

Due to the different values of T_1 for ^{29}Si in ZERODUR, when a 90° pulse was used, an interval of five times of the longest T_1 between the successive pulses is needed to recover the magnetization of sample to full equilibrium so that the quantitatively reliable spectra can be obtained. In the present case the recycle time has to be longer than 80 minutes. Considering the low sensitivity of Si NMR spectra it is

very time consuming to obtain a ^{29}Si NMR spectrum with desirable S/N ratio. In order to shorten the data taking time and still obtain quantitatively reliable spectra, a small flip angle and a short recycle time was used in experiments.

The change of the z component of magnetization of a sample in a magnetic field, dM, satisfies the following differential equation:

$$dM = (Meq - M)dt'/T_1$$

Its solution is

$$(Meq - M) = Cexp(-t'/T_1)$$

As above, after a $\theta°$ pulse the y component of the magnetization, My, is $M_0\sin(\theta)$, and the z component, Mz, is $M_0\cos(\theta)$. When successive pulses with recycle time t are applied, the M_0 will be stable at a certain value. When $t' = 0$ (just after a pulse), $Mz = M_0\cos(\theta)$ and when $t' = t$ (just before a pulse), $Mz = M_0$. Substituting these into above solution, we have

$$M_0 = Meq\ [1 - \exp(-t/T_1)]\ /\ [1 - \cos(\theta)\exp(-t/T_1)]$$

For example, When the flip angle is 45° and the repetition rate is 50 seconds, the height of peak with T_1 of 300 sec is 38% of its H_{eq} while that of 900 sec is 16% of its H_{eq}. The relative distortion is more than 50%. When the flip angle is 45° and the repetition rate is 900 seconds, the relative distortion is about 15%. When θ is small enough and t is long enough (still much shorter than $5T_1$), the ratios M_0/Meq

are very close to 1 for species with different T_1, meaning that the Mz of the sample before applying the pulses is close to Meq. So minimizing the distortion to an acceptable level is simple. For example, at a flip angle of 4° and a repetition rate of 50 seconds, the worst relative distortion between species with longest and shortest T_1's is about 3%. As a result the obtained spectrum is quantitatively reliable. Figure 12 shows the spectrum of ZERODUR taken with 4 degree pulses and 50 second recycle time. Table 3 shows the fitting results. It can be seen that the relative intensity of the broad peak was reduced and others were increased.

The ^{29}Si nucleus is spin 1/2. The anisotropic shielding can be averaged to zero by MAS and given the isotopic abundance of ^{29}Si (4.7%), Si-Si and Si-Al internuclear distances expected in aluminosilicates, MAS at speeds greater than 1 KHz would be expected to completely narrow both homo- and hetero-nuclear dipolar broadening. Therefore, in aluminosilicate systems which are highly ordered, narrow, liquid like lines are expected for ^{29}Si NMR spectra of powdered samples under MAS. In an aluminosilicate glass ceramics where the local environment of a majority of the Si atoms is tetrahedral, there is disorder in the second and succeeding coordination spheres and there is a dispersion of shielding anisotropies of Si. Under MAS the residual NMR linewidth will reflect this dispersion and the spectrum will be inhomogeneously broadened. The broadest peaks in both spectra inferred from the spectral fit cover almost the entire range of the four sharper peaks and imply a continuous variation in environment of the ^{29}Si atom. A spectrum which is a superposition of relatively sharp and broader

lines implies that the system is a mixture of ordered and relatively disordered regions.

A remaining question is whether this broad peak represents a single species and is broadened by the disordered nature of glass or is a superposition of several peaks of which each peak represents a Si tetrahedral species, $Si(OAl)_n$, n=0,1,2,3,4. The broad peak can not be separated further. If this peak represents a single species, its first moment will not vary with the chemical composition of the glass ceramic sample. If this peak is a superposition of several peaks each of which represents a $Si(OAl)_n$ species, its chemical shift is a weighted average of these component peaks. When the chemical composition of the glass sample varies, the relative intensity of each component peak will vary and the weighted average value, the first moment of the broad peak, will vary too. As a comparison, the MAS NMR spectrum of another glass sample with similar structure but different chemical composition, called glass 2, was measured under the same conditions as that of ZERODUR. The spectrum and fit results are shown in Figure 13 and Table 4. The first moments of the broad peak in the two spectra are 101 and 104, respectively while other peaks remain unchanged. The difference of 3 ppm in the first moments in the two spectra indicates that this peak does not represent a single disordered chemical species, $Si(OAl)_n$, but may reasonably be taken to represent a superposition of several peaks of $Si(OAl)_n$ species. The disorder of $Si(OAl)_n$ units represented by the broad peak is so high that these peaks cannot be separated from each other.

In all aluminosilicates there appears to be a strong tendency according to Loewenstein's rule for each aluminum atom to be linked, via oxygen bridges, to four Si atoms, which means that the local environment of Al is always $Al(OSi)_4$. When the pulse recycle time in the experiments is long enough to allow all relevant nuclei to fully equilibrate and the peaks in the spectra are correctly assigned in terms of the various $Si(OAl)_n$ units, the Si/Al ratio of the aluminosilicate sample can be calculated directly from the spectrum using the following expression:

$$(Si/Al) = \frac{\sum_{n=0}^{4} I_{Si(OAl)n}}{\sum_{n=0}^{4} \frac{n}{4} I_{Si(OAl)n}}$$

Where $I_{Si(OAl)n}$ is the intensity of the NMR signal attributable to $Si(OAl)_n$ units. This equation is structure-independent and applies to all aluminosilicates provided that the assumptions made in its derivation are correct, i.e., that each sharp peak in the spectrum is associated with a different value of n (an assumption known not to be true for zeolites such as offretite). The value of Si/Al can therefore serve as a test for the correctness of spectral assignments. If it is assumed that the five $Si(OAl)_n$ species in the ordered and disordered regions have the same chemical shift, the average number of neighbor (OAl) of Si, n, in the disordered region can be obtained from the first moment of the broad peak due to a linear relation between the chemical

shifts and the number of neighboring Al, n. In this situation the n is not necessarily an integral. The above equation can still be used to calculate the value of Si/Al. The calculated value of Si/Al from NMR is 2.4 for ZERODUR and 3.0 for glass 2. Comparing to values from chemical analysis, 2.0 and 2.6, respectively, the difference is about 20%. This difference compares with similar values from quantitative NMR measurements of zeolites[101] by Corbin. It would thus appear that Loewenstein's rule is approximately obeyed in these two glasses.

The possible sources of error in the calculation of Si/Al from NMR are:

1. presence of inequivalent sites.
2. the Loewenstein rule is violated.
3. the assumption that each $^{29}Si(OAl)_n$ species in both ordered and disordered regions has identical chemical shift is not valid.
4. the existence of nonframework Al such as 6- or 5-coordinated Al.

The existence of 6- or 5-coordinated Al can be excluded from the high resolution Al NMR spectra(see below). Also, Al NMR spectra shows that there exists two geometrically different sites in the two glass-ceramic samples. The site in the highly ordered region has a symmetry roughly cubic. The other, in a relatively disordered region exhibits a spectrum indication of axial symmetry. As a result, ^{29}Si atoms at the two sites may have different chemical shifts, and the main source of error may be the invalidity of the assumption that the chemical shifts of each $Si(OAl)_n$ species in both ordered and disordered regions are identical. This assumption is acceptable only as a zero order

approximation. The approximate agreement between NMR and chemical analysis implies that the Loewenstein rule is probably obeyed in both regions.

^{27}Al MAS NMR spectra of aluminosilicate glasses could be much simpler than their ^{29}Si counterparts. If Loewenstein's rule holds, only one type of $Al(OSi)_4$ environment is possible for the aluminum atom, while five possibilities exist for the silicon. But all Si atoms in framework aluminosilicates are 4-coordinated, while Al atoms can be 4-, 5- and 6-coordinated. The ^{27}Al MAS NMR is a very sensitive probe for the coordination of Al.

The high resolution Al NMR spectra of the two samples are shown in Figures 14-17. Figures 14 and 15 were taken at 57 MHz, and Figure 16 and 17 were taken at 77 MHz. Comparing these spectra taken at 77 MHz and at 57 MHz, some interesting differences can be seen:

(1) The highest point of the peaks are around -50 ppm. So these peaks represent the four coordinated ^{27}Al in the two glasses. The locations of the steps in middle of peaks vary with the increasing magnetic field from 16 ppm to 25 ppm for ZERODUR and from 13 ppm to 26 ppm for glass 2. In addition these steps do not appear around 32 ppm. So the steps are not peaks representing the 5-coordinated ^{27}Al in glasses. They are part of the peak of four coordinated ^{27}Al. The lack of a peak at 0 ppm implies there is no 6- coordinated ^{27}Al present. As a result, only four coordinated Al is inferred to be present. It is possible that five or six coordinated aluminum is present in a form so disordered as to result in an NMR spectrum broadened out of the observation range of our spectrometer. Such a result would be in

accord with the values of Si/Al inferred from NMR vs those from chemical analysis.

(2) Comparing with the theoretical line shape associated with the quadrupole interaction, the line shape of the central transition of the ^{27}Al MAS NMR spectra at 57 MHz indicates that there is a species in the sample for which the electric field gradients (EFG) tensor is nearly axially symmetric, $\eta=0$. Also the relative heights of the two observed peaks indicates that this spectrum is a superposition of two peaks, one associated with a value $\eta=0$ and another with a symmetric Gaussian like line shape. As a result, there are two species being observed under the downfield peak. In addition, the spectrum indicates that the aluminum being observed is in a highly ordered material. If not, the two peaks would be considerably broader than observed.

(3) If the MAS NMR spectrum of a half integral quadrupole nuclear spin in a powdered sample is mainly broadened by the second order quadruple interaction, the line width of the $1/2 \Leftrightarrow -1/2$ transition, measured in Hz, is inversely proportional to the magnetic field and the spectrum will be narrowed by increasing magnetic field. On the other hand, if the spectrum is mainly broadened by chemical shift dispersion associated with disorder in the structure, the line shape is the envelope of all peaks of a given species with slightly different chemical shifts due to the structural disorder. The line width of the central transition will then be proportional to the magnetic field, i.e., the spectrum will be broadened by increasing magnetic field. In the two ^{27}Al MAS NMR spectra of glasses at 57 and 77 MHz, the line widths decrease slightly from 4.272 KHz to 4.028 KHz and are nearly

identical. This result implies that both effects of quadrupole interaction and broadening of structural disorder are simultaneously present: (a) the effect of the EFG on on both lines present is decreased as the field is raised, and (b) the dispersion due to structure disorder increases as the field is raised. The result is a slightly reduced total line width, not inversely proportional to the magnetic field. In the spectrum at 77 MHz, the two peaks appearing in the spectrum of 57 MHz merge together. This result indicates that these two peaks are part of a spectrum associated with an axially symmetric EFG.

(4) Both NMR spectra of ^{27}Al of ZERODUR and of glass 2 under MAS at 77 MHz show a peak, which does not appear in the spectrum of 57 MHz, at the tip of the peak. The existence of the small peak further confirms the above observations. There are two chemical shifted Al peaks representing two distinct types of four coordinated framework sites occupied by the aluminum. One is highly ordered and in a nearly cubic symmetrical environment; $e^2qQ \sim 0$. This peak appears at higher field and is not smeared by structural disorder. This result indicates that the quadrupole interaction is dominant and structural disorder is not important for this type of tetrahedral site. The other is relatively less highly ordered and with an axially symmetrical EFG, $\eta=0$. The fact that the two major peaks which appear in the low field spectrum merge in the higher field spectrum confirms the identity of the up-field shoulder as being part of the central transition of a quadrupole species in a nearly axial EFG. The above results are consistent with

the inference from the ^{29}Si MAS NMR spectra that there are two regions, ordered and relatively disordered, existing in the two glass samples.

(5) The NMR spectrum of ^{27}Al of ZERODUR sample under MAS was measured at 130.3 MHz with a result similar to that of spectrum at 77 MHz. Figure 18 shows the spectrum. The peak is at 47 ppm and there are no peaks around 0 ppm and 33 ppm. The entire peak width is reduced to 2.867 KHz. Two peaks appear at the top of the spectrum.

CONCLUSIONS

The NMR studies of the two samples of glass ceramics show that:

(a) Both glasses are highly ordered materials.

(b) There are two regions in the two glasses. Si and Al atoms in the two regions are tetrahedrally coordinated. One of the regions is a highly ordered crystalline like region. The Si and Al sites in the region have a cubic symmetry environment. As a result, the MAS NMR of ^{29}Si in this area is similar to that of aluminosilicate zeolites. The quadrupole interaction of ^{27}Al in the region is close to zero. The other is a relatively disordered region. Si and Al atoms in this region have an axially symmetry environment. The ^{27}Al spectrum shows a quadrupole powder pattern with an asymmetry parameter $\eta \approx 0$.

(c) The Loewenstein rule is basically obeyed in both samples.

(d) No 5- or 6-coordinated Al found in the two samples.

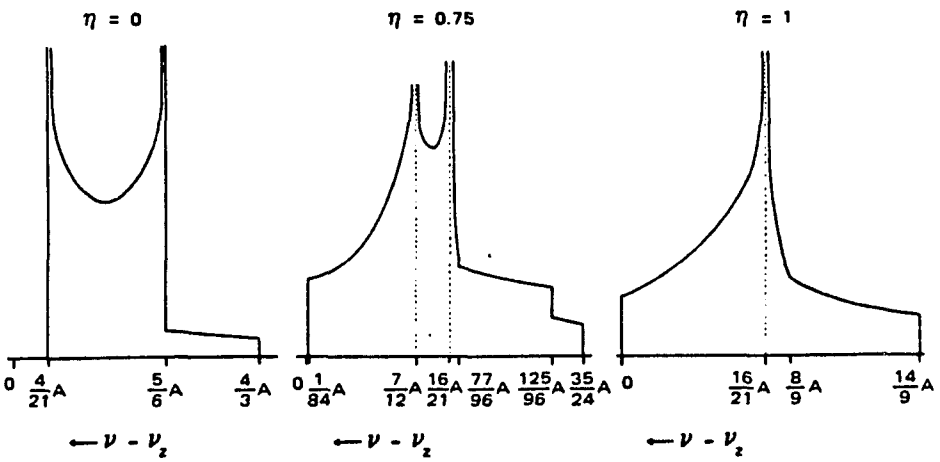

Figure 1. Theoretical quadrupole powder patterns. [Theoretical line shape of the -1/2⟷1/2 transition of a quadrupolar nuclear spin in a powder with fast MAS for different values of the asymmetry parameter η [91]]

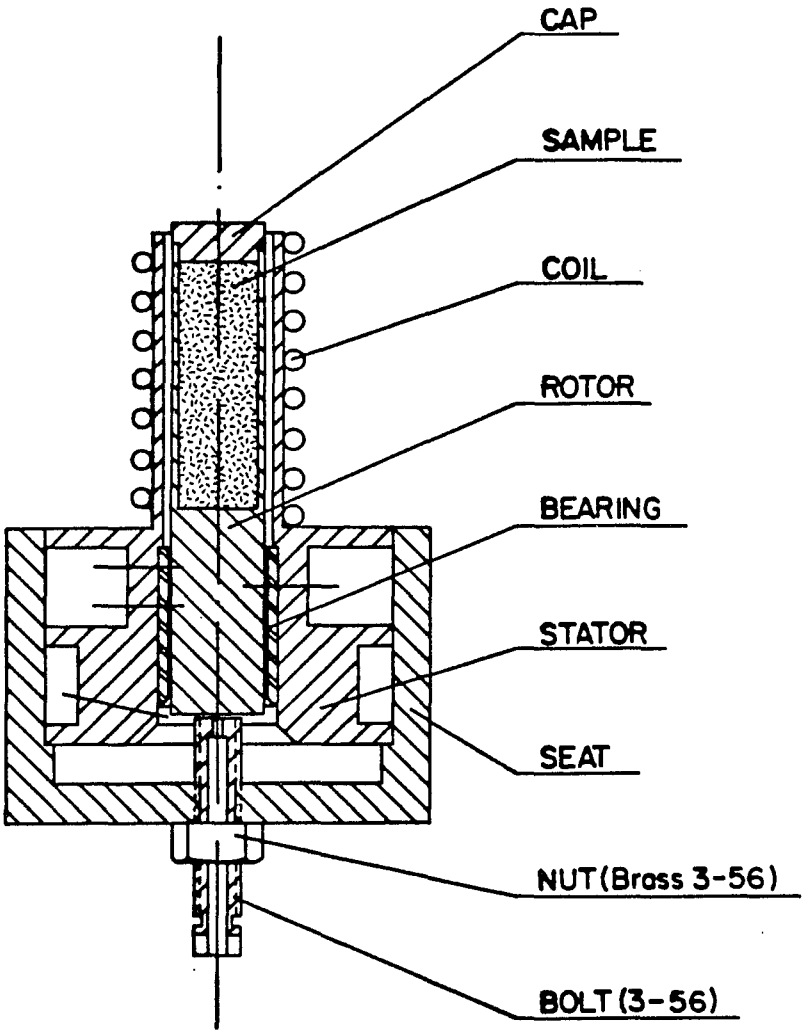

Figure 2. Spin system assembly

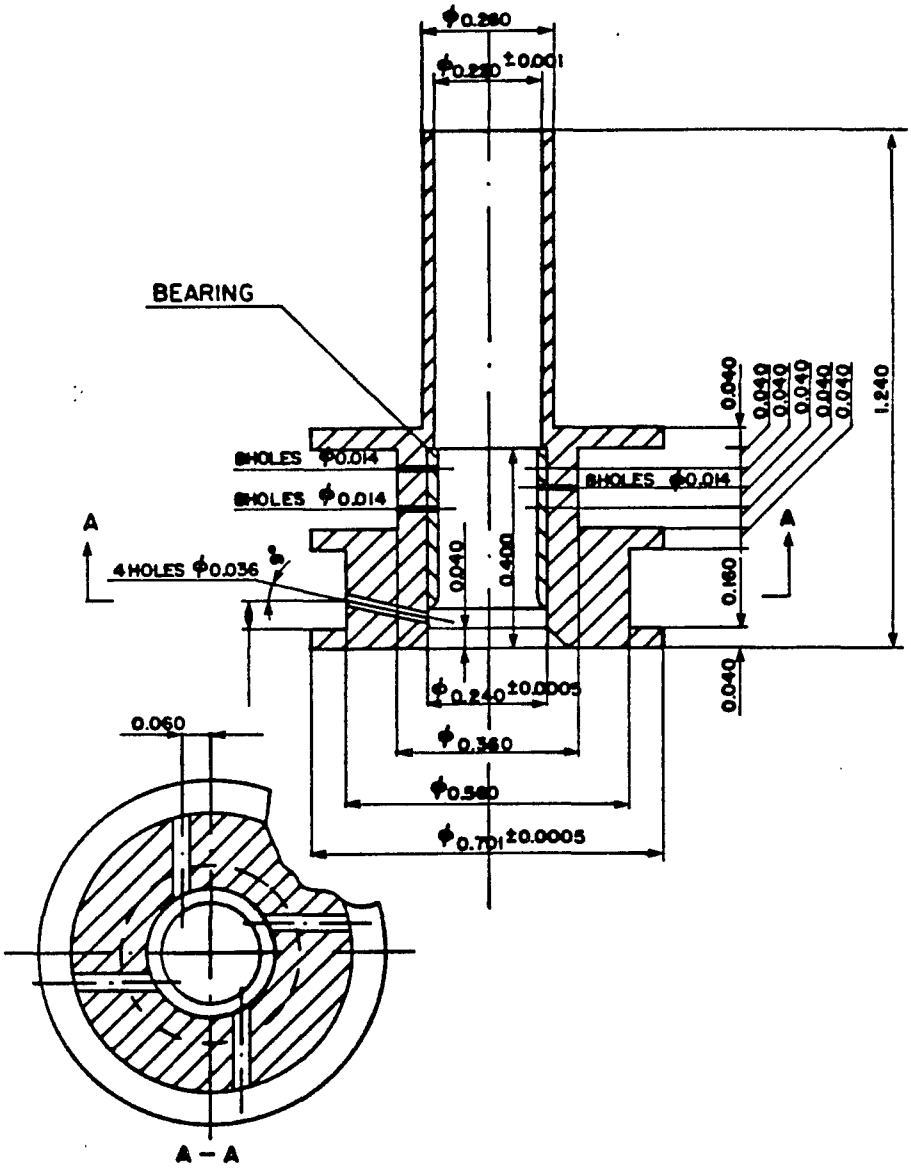

Figure 3. Stator and air bearing ring

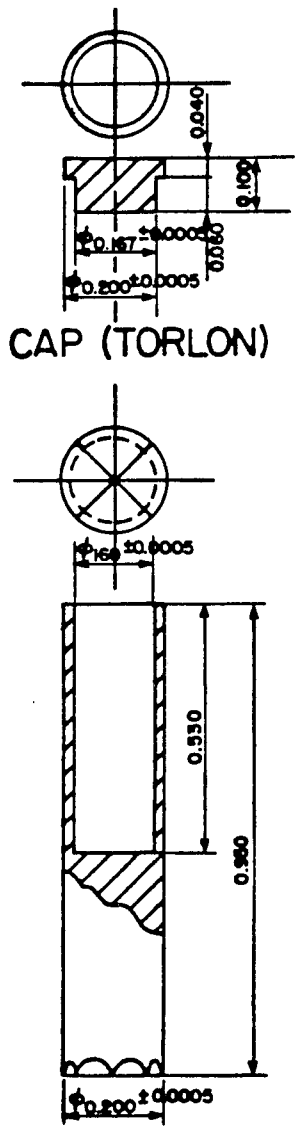

Figure 4. Rotor

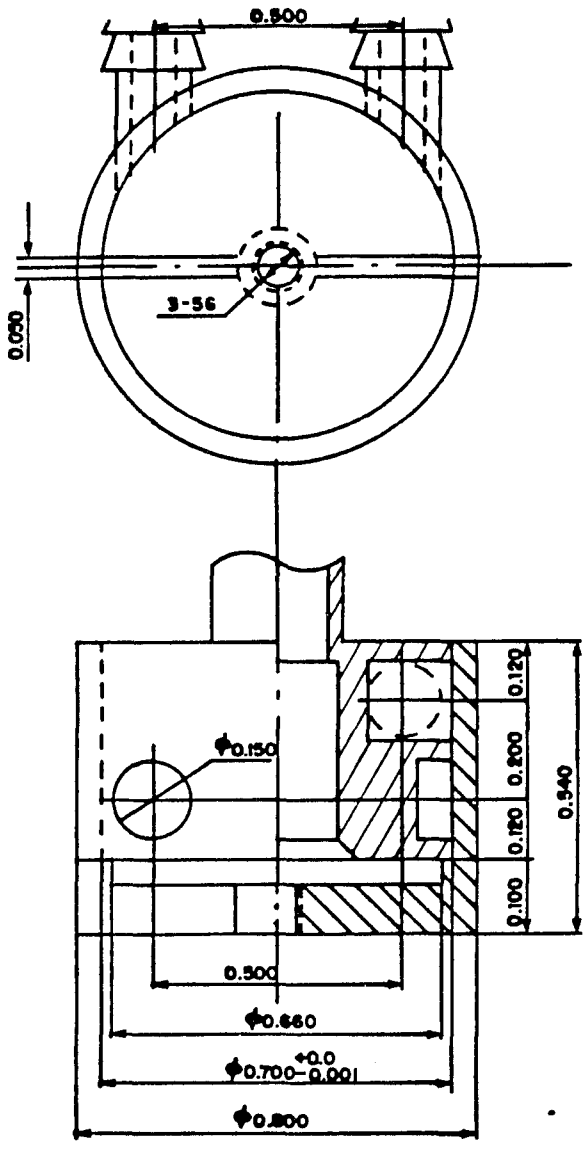

Figure 5. Stator seat and stator

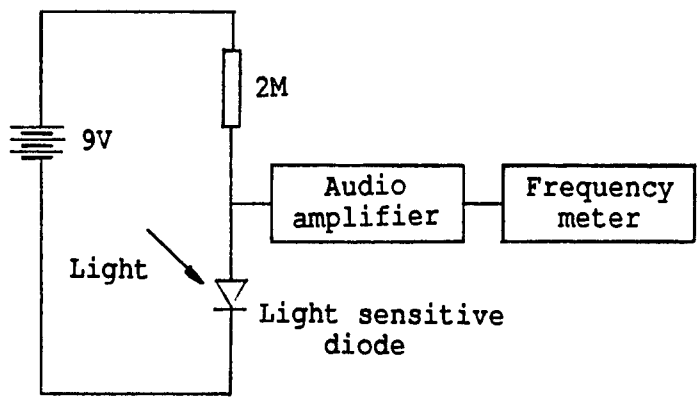

Figure 6. The circuit for spinning speed measurement

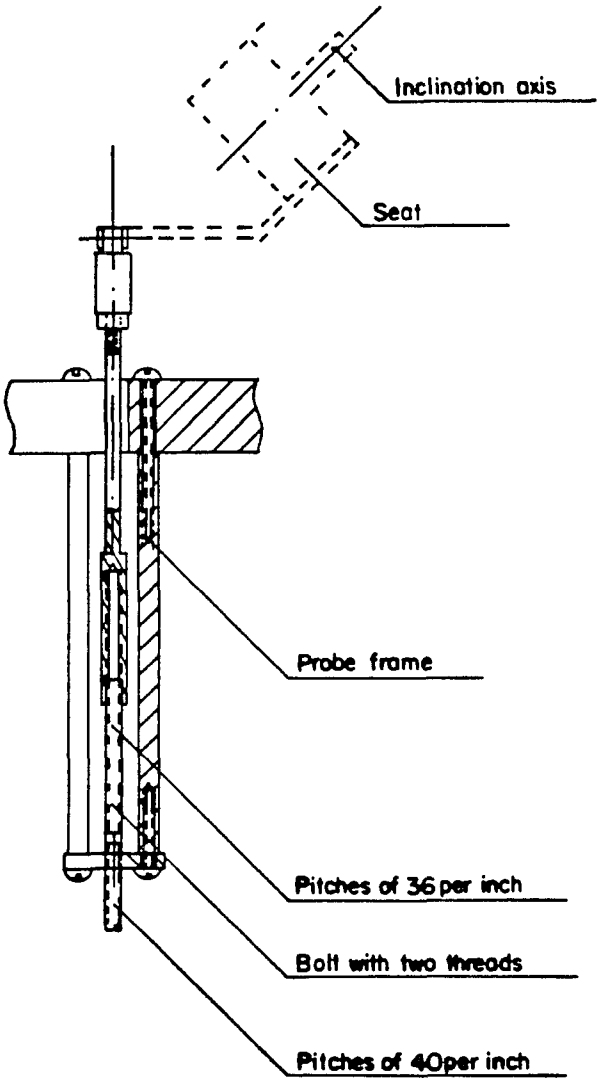

Figure 7. Magic angle adjustment

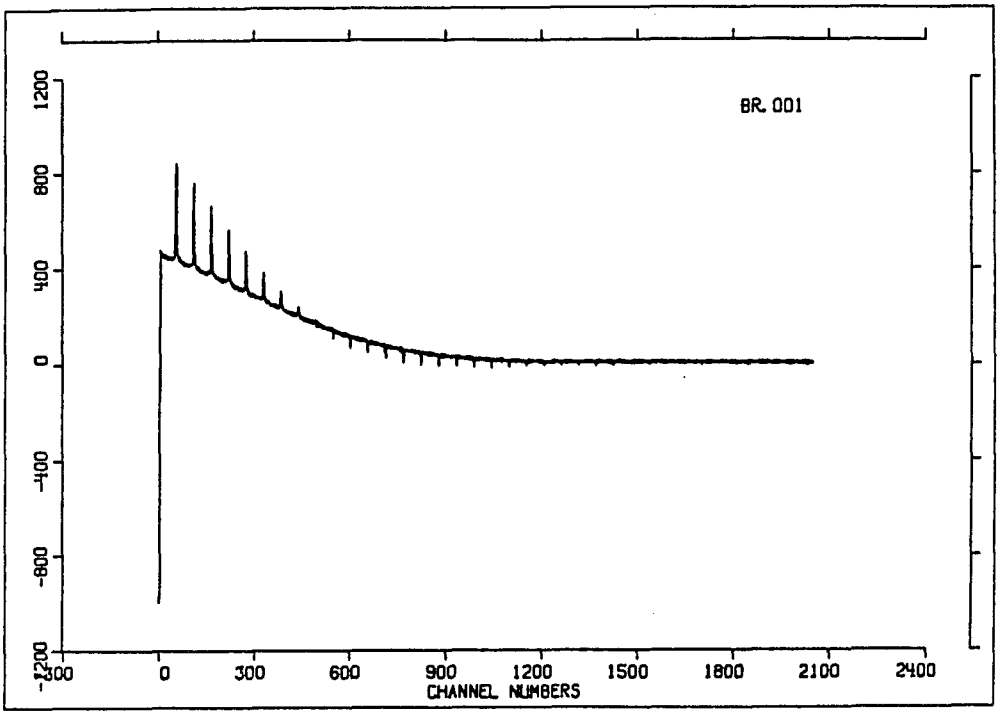

Figure 8. Rotational echos of ^{79}Br in KBr at magic angle

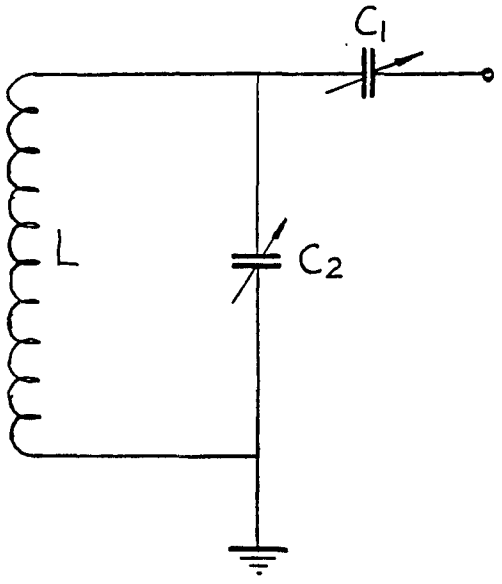

Figure 9. The probe circuit

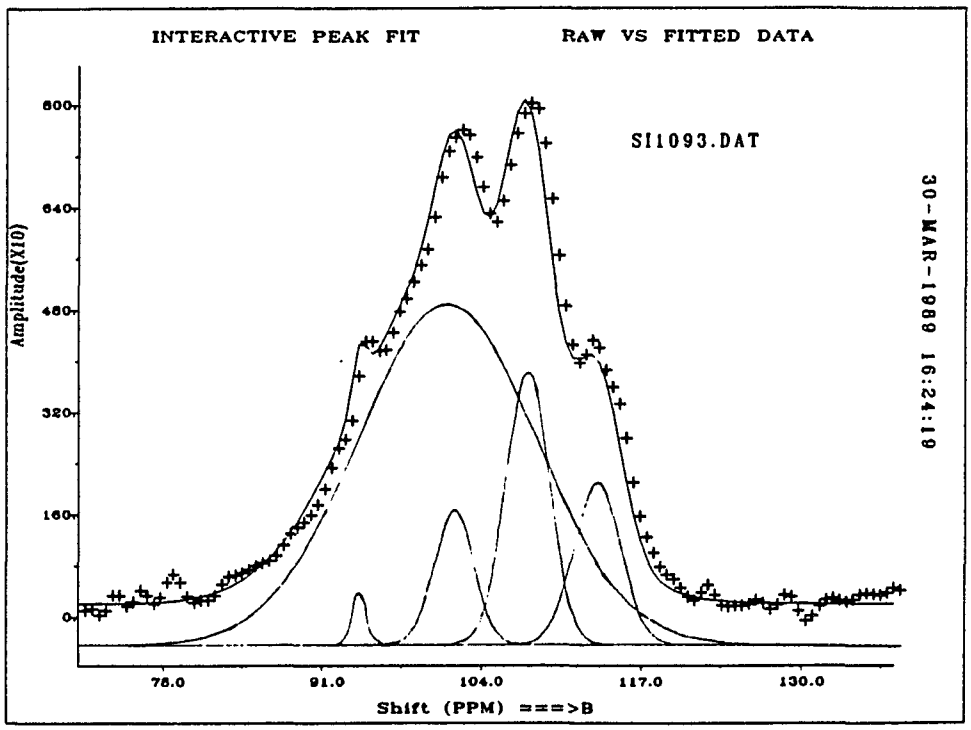

Figure 10. MAS NMR spectrum of ZERODUR taken with 90 degree pulse and 700 seconds recycle time

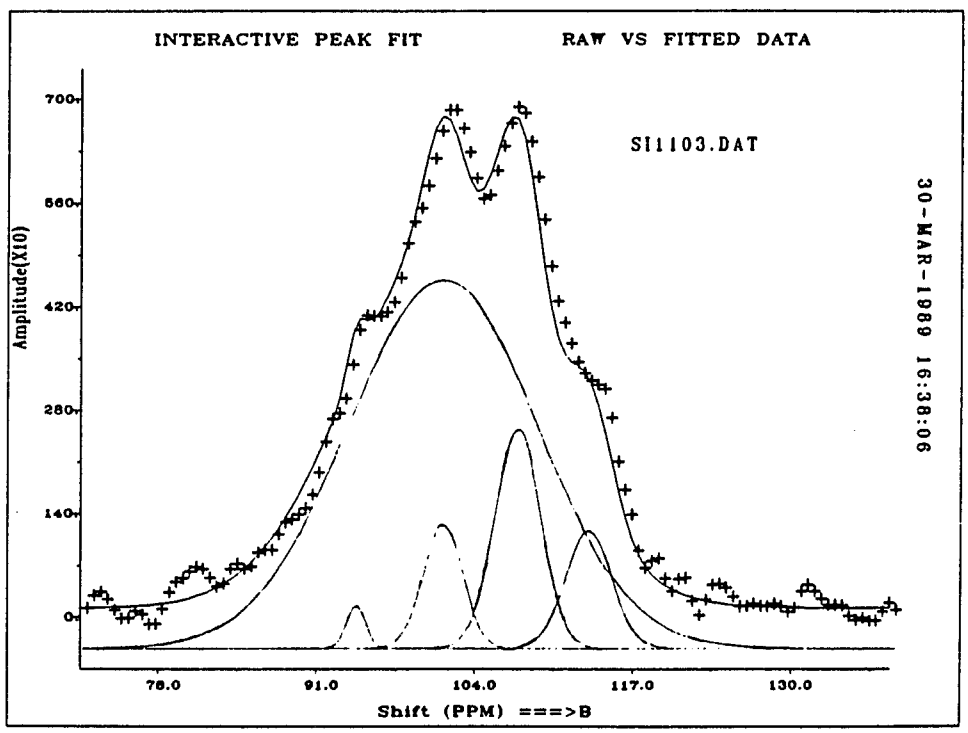

Figure 11. MAS NMR spectrum of ZERODUR taken with 90 degree pulse and 200 seconds recycle time

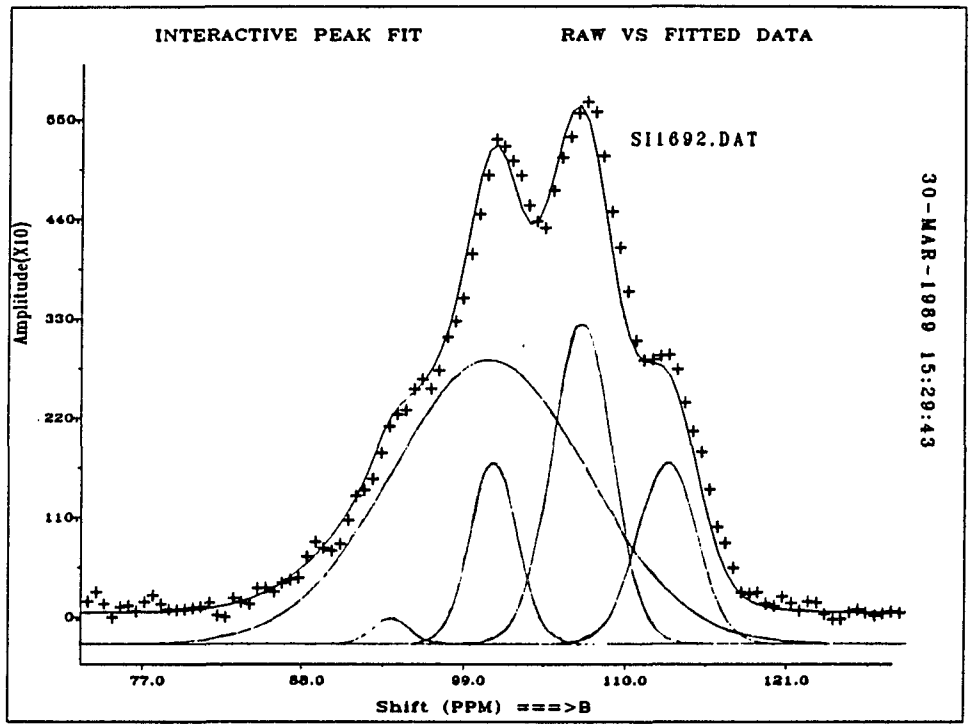

Figure 12. MAS NMR spectrum of ZERODUR taken with 4 degree pulse and 50 second recycle time

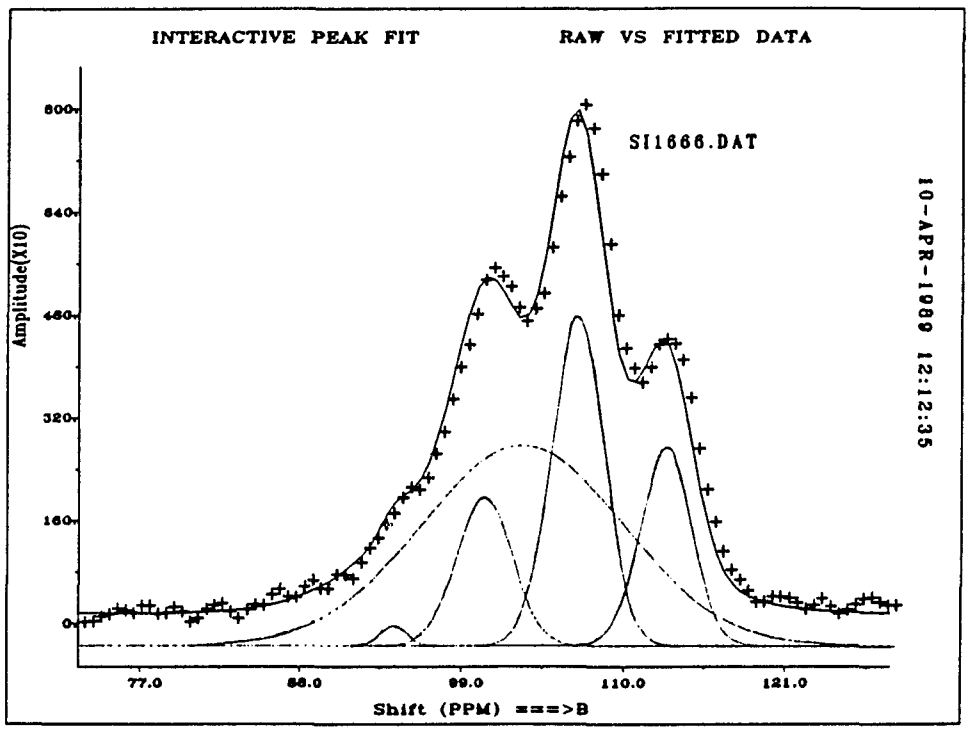

Figure 13. MAS NMR spectrum of glass 2 taken with 4 degree pulse and 50 seconds recycle time

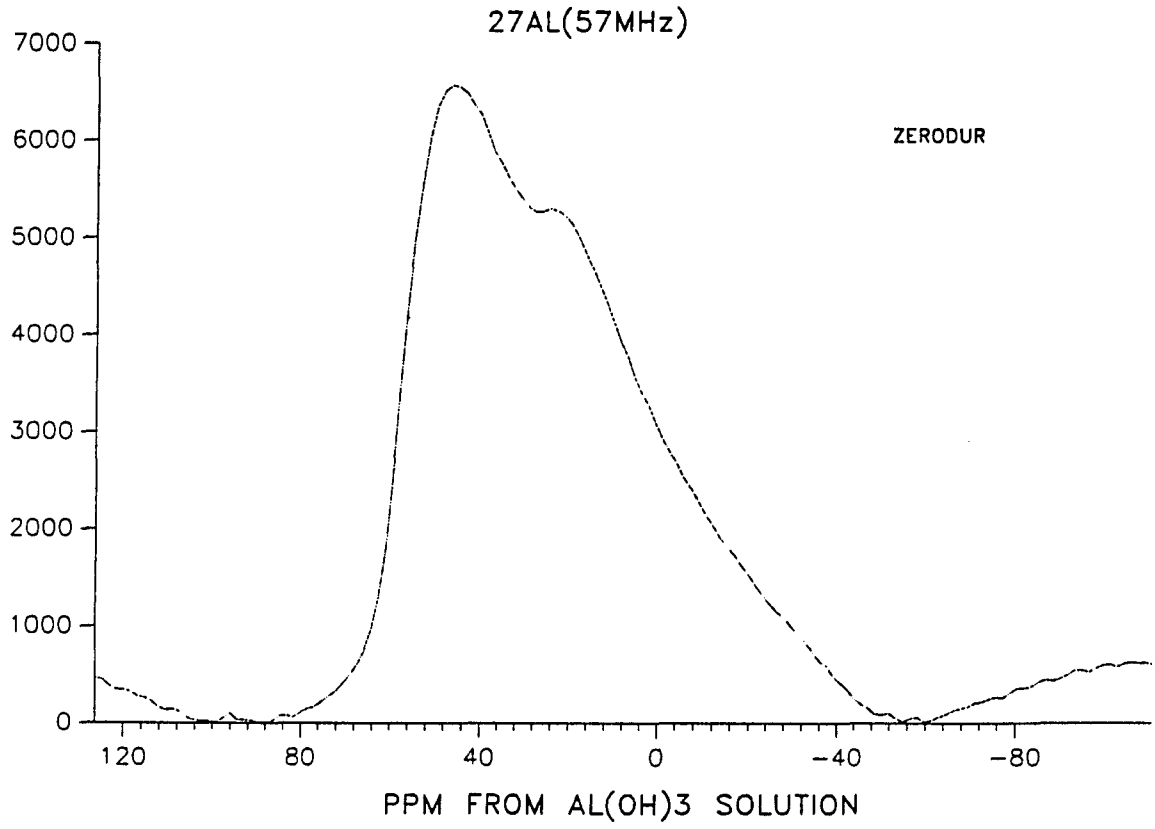

Figure 14. ^{27}Al MAS NMR spectrum of ZERODUR taken at 57 MHz

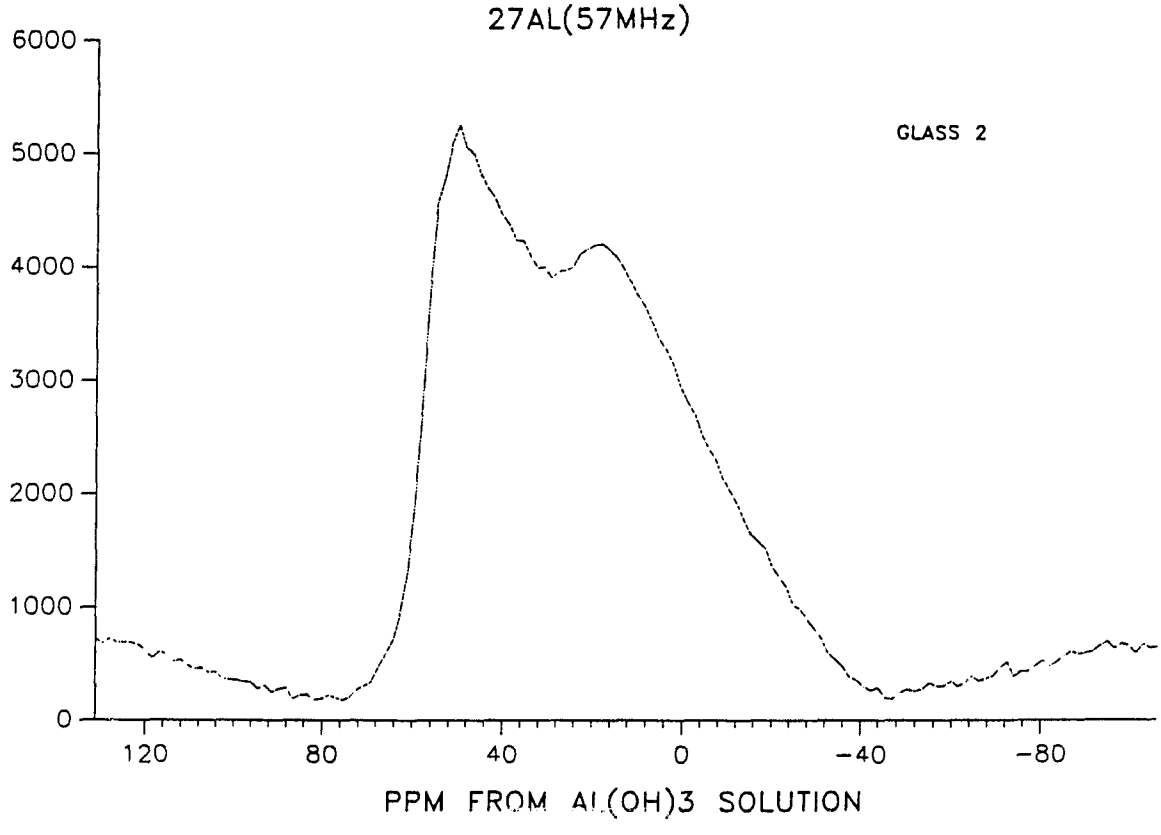

Figure 15. ^{27}Al MAS NMR spectrum of glass 2 taken at 57 MHz

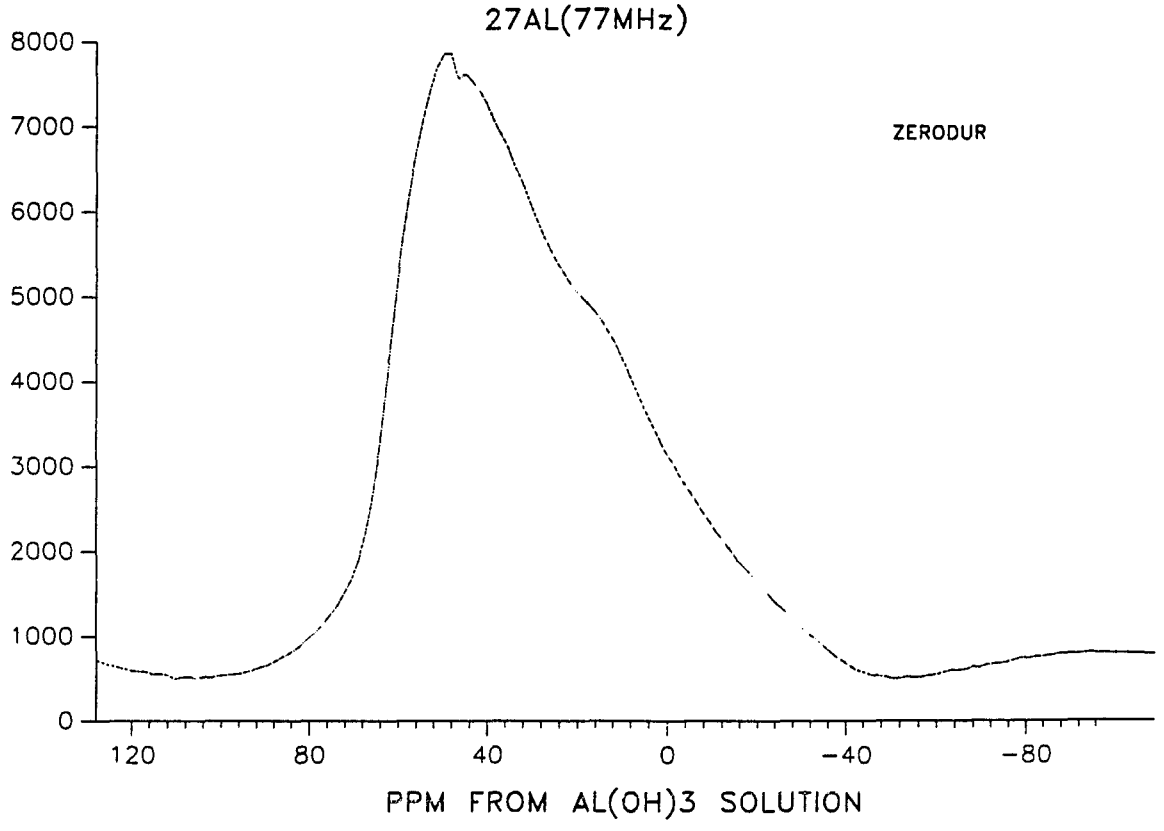

Figure 16. ^{27}Al MAS NMR spectrum of ZERODUR taken at 77 MHz

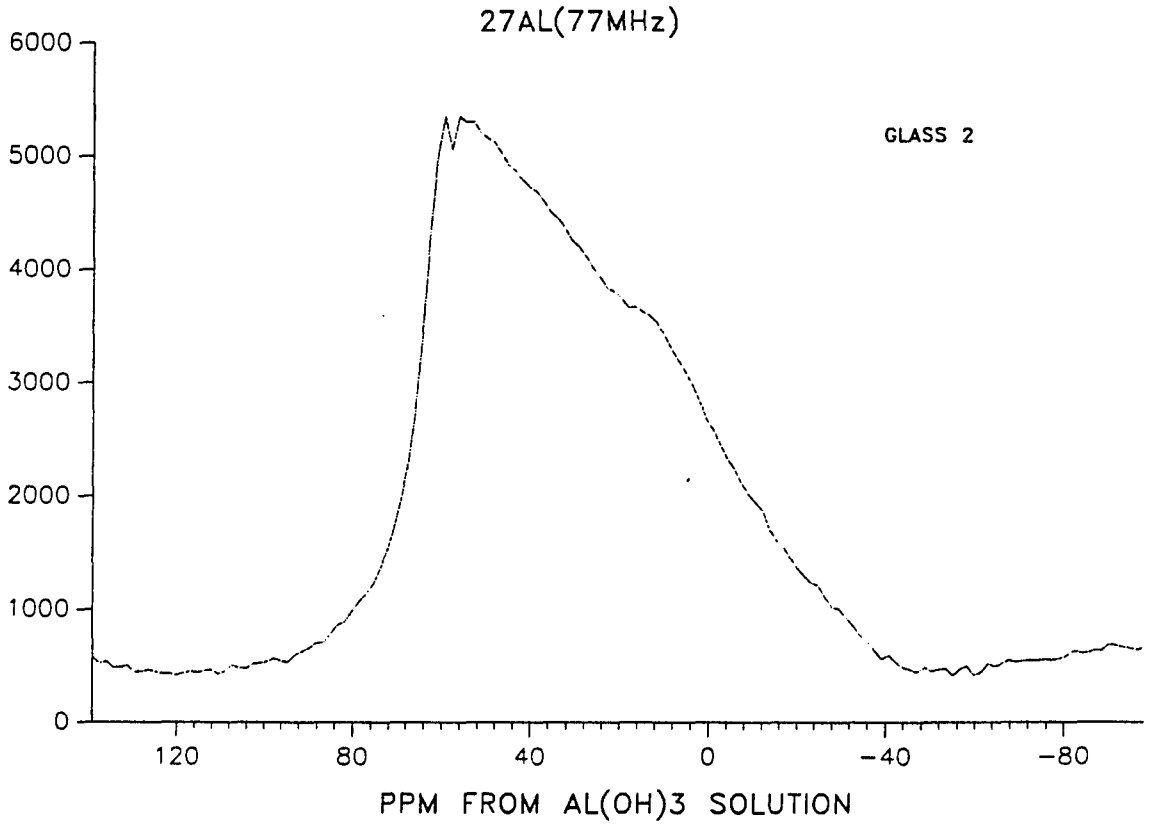

Figure 17. ^{27}Al MAS NMR spectrum of glass 2 taken at 77 MHz

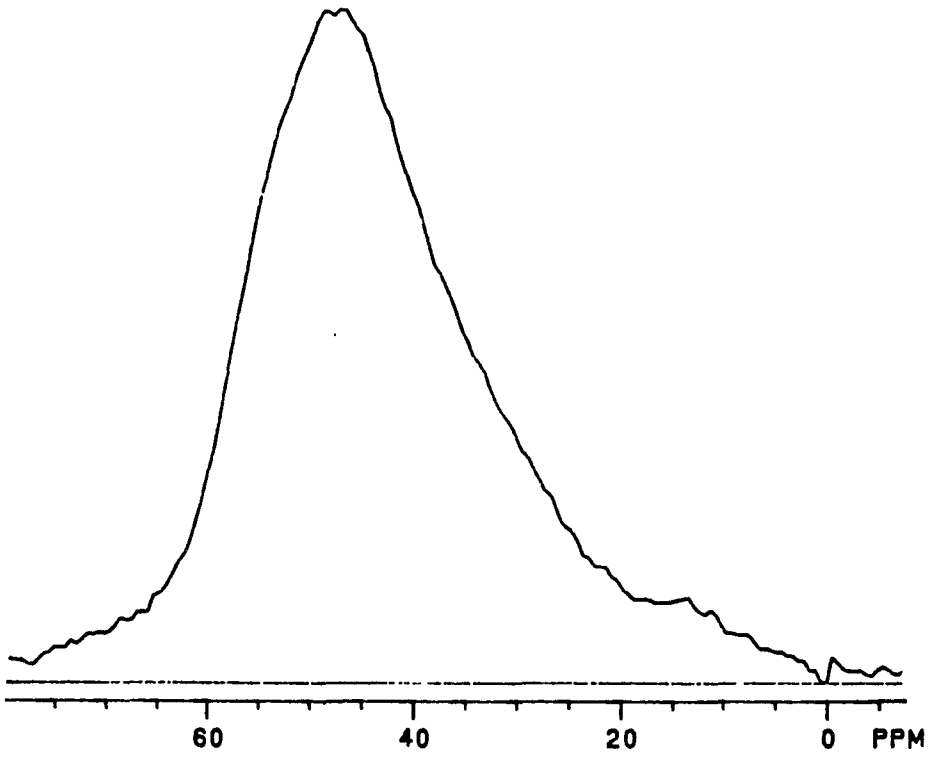

Figure 18. ^{27}Al MAS NMR spectrum of ZERODUR taken at 130 MHz

Table 1. Fit parameters for the ^{29}Si NMR spectrum of ZERODUR taken with a recycle time of 700 seconds

Peak	Maximum height	Full width(ppm)	Shift(ppm)
1	2524.1	4.49	113.5
2	4257.7	4.13	107.7
3	2101.0	3.75	101.8
4	5313.4	17.02	101.2
5	802.0	1.40	94.5

Table 2. Fit parameters for the ^{29}Si NMR spectrum of ZERODUR taken with a recycle time of 200 seconds

Peak	Maximum height	Full width(ppm)	Shift(ppm)
1	906.1	4.46	113.4
2	1689.8	4.44	107.5
3	949.5	3.80	101.4
4	2844.8	18.16	101.3
5	327.1	1.79	92.3

Table 3. Fit parameters for the ^{29}Si NMR spectrum of ZERODUR taken with a recycle time of 50 seconds and a flip angle of 4 degree

Peak	Maximum height	Full width(ppm)	Shift(ppm)	Percent area
1	1991.8	4.80	113.1	11.40
2	3535.7	4.79	107.3	20.20
3	1997.9	3.80	101.3	9.06
4	3126.0	15.66	101.0	58.41
5	281.6	2.77	94.3	0.93

Table 4. Fit parameters for the ^{29}Si NMR spectrum of Glass 2 taken with a recycle time of 50 seconds and a flip angle of 4 degree

Peak	Maximum height	Full width(ppm)	Shift(ppm)	Percent area
1	3075.4	4.12	113.4	13.32
2	5116.8	4.17	107.4	22.45
3	2294.2	4.47	101.1	10.81
4	3112.9	16.09	103.6	52.73
5	304.4	2.16	94.9	0.69

REFERENCES

1. C. A. Fyfe, "Solid State NMR for Chemists"; CFC Press: Guelph, Ontario, Canada, 1983.

2. J. M. Thomas and J. Klinowski, Advance in Catalysis, Vol. 33, p.199.

3. E. R. Andrew and V. T. Wynn, Proc. R. Soc. London Ser. A, **291**, 257 (1966).

4. V. M. Goldschmidt, Skrifter Norske Videnskaps Akad. (Oslo), Mat.-natur., **1**(8), 7 (1926).

5. H. Zachariasen, J. Am. Chem, Soc., **54**, 3841 (1932).

6. B. E. Warren, H. Krutter, and O. Morningstar, J. Am. Ceram. Soc., **19**, 202 (1936).

7. W. L. Bragg, The Structure of Silicates. Acad. Publ. Soc., Leipzig, LK1930; reviewed in Z. Krist., **74**, 237 (1930); Ceram. Abstr., **10**[1] 73 (1931); J. Soc. Glass Technol., **14**, 295 (1930).

8. R. L. Mozzi and B. E. Warren, J. Appl. Crystallogr., **2**, 164 (1969).

9. F. Ordway, Science, **143**, 800 (1964).

10. D. L. Evans and S. V. King, Nature, **212**, 1353 (1966).

11. R. J. Bell and P. Dean, Nature, **212**, 1354 (1966).

12. M. Hass, J. Phys. Chem. Solids, **31**, 415 (1970).

13. A. J. Leadbetter, J. Chem. Phys., **51**, 779 (1969).

14. R. J. Bell and P. Dean, Disc. Far. Soc., **50**, 55 (1970).

15. J. F. Randall, H. R. Rooksby, and B. S. Cooper, J. Soc. Glass Technol., **14**, 219 (1930).

16. N. Valenkov and E. Porai-Koshitz, Z. Krist., **45**, 195 (1936).

17. B. E. Warren and J. Briscoe, J. Am. Ceram. Soc., **21**, 49 (1938).

18. A. H. Narten, J. Chem. Phys., **56**, 1905 (1972).

19. J. H. Konnert and J. Karle, Nature Phys. Sci., **236**, 92 (1972).

20. L. W. Tilton, J. Res. Nat. Bur. Stand., **59**, 139 (1957).

21. H. A. Robinson, J. Phys. Chem. Solids, **26**, 209 (1965).

22. R. J. Bell and P. Dean, Phys. Chem. Glass, **9**, 125 (1968); **10**, 164 (1969).

23. J. D. McConnell, Mineral Soc. Am., **14**, 165 (1985).

24. R. J. Bell and P. Dean, Phil. Mag., **25**, 1381 (1972).

25. R. Zallen, "The Physics of Amorphous Solids"; John-Wiley & Sons: New York, 1983.

26. E. Machatschki, Zbl. Min. Geol. Pal., (A) 136 (1934); Z. Krist, Strukturbericht III, 546.

27. T. F. W. Barth, Am. J. Sci., (5) **27**, 273 (1934).

28. W. Loewenstein, Am. Mineral., **39**, 92 (1954).

29. S.Ramdas and J. Klinowsky, Nature, **308**, 521 (1984).

30. A. -R. Grimmer, F. von Lampe, M. Magi and E. Lippmaa, Monatshefte fur Chemie, **114**, 1053 (1983).

31. A. -R. Grimmer, F. von Lampe, M. Magi and E. Lippmaa, Monatshefte fur Chemie, **115**, 561 (1984).

32. A. -R. Grimmer and R. Radeglia, Chem. Phys. Letters, **106**, 262 (1984).

33. S. A. Brawer and W. B. White, J. Chem. Phys., **63**, 2421 (1975).

34. B. O. Mysen, D. Virgo and F. A. Seifert, Rev. Geophys., **20**, 353 (1982).

35. P. McMillean, Am. Mineral., **69**, 622 (1984).

36. D. W. Matson, S. K. Sharma and J. A. Philpotts, J. Non-Crystallogr. Solids, **58**, 323 (1983).

37. I. A. Harris and P. J. Bray, Phys. Chem. Glasses, **21**, 156 (1980).

38. P. McMillan and B. Pirion, J. Non-Crystallogr. Solids, **53**, 279 (1980).

39. K. Kusabiraki and Y. Shiraishi, J. Non-Crystallogr. Solids, **44**, 365 (1981).

40. A. Navrotsky, K. L. Geisinger, P. McMillan and G. V. Gibbs, Phys. Chem. Minerals, **11**, 284 (1985).

41. M. Taylor and G. E. Brown, Geochim. Cosmochim. Acta, **43**, 61 (1979).

42. M. Taylor and G. E. Brown, Geochim. Cosmochim. Acta, **43**, 1467 (1979).

43. Y. Waseda, "The Structure of Non-Crystalline Materials"; McGraw-Hill: New York, 1980.

44. B. H. W. S. de Jong and G. E. Brown, Geochim. Cosmochim Acta, **44**, 1627 (1980)

45. B. D. Mosel, W. Muller-Warmuth and H. Dutz, Phys. Chem. Glasses, **15**, 154 (1974).

46. G. R. Holzman, P. C. Lauterbur, J. H. Anderson and W. Koth, J. Chem. Phys., **25**, 172 (1956).

47. M. G. Gibby, A. Pines and J. S. Waugh, J. Am. Chem. Soc., **94**, 6231 (1972).

48. E. Lippmaa, M. Alla, T. J. Pehk and G. Engelhardt, J. Am. Chem. Soc., **100**, 1929 (1978).

49. E. Lippmaa, M. Magi, A. Samoson, G. Engelhardt and A. -R. Grimmer, J. Am. Chem. Soc., **102**, 4889 (1980).

50. M. Magi, E. Lippmaa, A. Samoson, G. Engelhardt and A. -R. Grimmer, J. Phys. Chem., **88**, 1518 (1984).

51. E. Lippmaa, M. Magi, A. Samoson, M. Tarmak and G. Engelhardt, J. Am. Chem. Soc., **103**, 4992 (1981).

52. G. Engelhardt, U. Lohse, E. Lippmaa, M. Tarmak and M. Magi, Z. Anog. Allg. Chem., **482**, 49 (1981).

53. J. M. Thomas, C. A. Fyfe, S. Ramdas, J. Klinowski and G. C. Gobbi, J. Phys. Chem., **86**, 3061 (1982).

54. J. Klinowski, J. M. Thomas, S. Ramdas, C. A. Fyfe and G. C. Gobbi, "Second Workshop on the Adsorption of Hydrocarbons in Microporous Sorbents"; Eberswalde, G. D. R.: November 1982, Vol. 2, supplement.

55. J. Klinowski, S. Ramdas, J. M. Thomas, C. A. Fyfe and J. S. Hartman, J. Chem. Soc. Faraday Trans. II, **78**, 1025 (1982).

56. V. Gramlich and W. M. Meier, Z. Kristallogr., **133**, 134 (1971).

57. J. J. Pluth and J. V. Smith, J. Phys. Chem., **83**, 741 (1969).

58. M. T. Melchior, D. E. W. Vaughan, R. H. Jarman and A. J. Jacobson, Nature (London), **298**, 455 (1982).

59. C. A. Fyfe, G. C. Gobbi, G. J. Kennedy, C. T. DeSchutter,W. J. Murphy, R. S. Ozubko and D. A. Slack, Chem. Lett., 163 (1984).

60. C. A. Fyfe, G. C. Gobbi, W. J. Murphy, R. S. Ozubko and D. J. Slack, J. Am. Chem. Soc., **106**, 4435 (1984).

61. J. M. Thomas, J. Klinowski, S. Ramdas, B. K. Hunter and D. T. B. Tennakoon, Chem. Phys. Lett., **102**, 158 (1983).

62. M. T. Melchior, D. E. W. Vaughan and A. J. Jacobson, J. Am. Chem. Soc. **104**, 4859 (1982).

63. J. B. Murdoch, J. F. Stebbins and I. S. E. Carmichael, Am. Miner., **70**, 332 (1985).

64. Y. Ohashi and L. W. Finger, The effect of Ca substitution on the Structure of clinoenstatite, Carnegie Institution of Washington Year Book, **75**, 743 (1976).

65. J. H. Iwamiya and B. C. Gerstein, Zeolites, **6**, 181 (1986).

66. R. D. Farlee, D. R. Corbin and A. J. Vega, presented in part at the Rocky Mountain Conference, Denver, CO, Aug., 1983.

67. R. D. Farlee, and D. R. Corbin, presented in part at the International Chemical Congress of Pacific Basin Societies, Honolulu, HI, Dec., 1984.

68. A. Samson, E. Lippmaa, and N. C. M. Alma, Bruker Rep., **1**, 14 (1984).

69. E. Oldfield, S. Samoson, M. D. Meadows, K. A. Smith, R. A. Kinsey and J. Ackerman, J. Am. Chem. Soc., **104**, 919 (1982).

70. S. Ganapathy, S. Schramm and E. Oldfield, J. Chem. Phys., **77**, 4360 (1982).

71. J. W. Akill, N. N. Greenwood, B. L. Khandelwal and G. D. Lester, J. Chem. Soc. Dalton Trans., 604 (1972).

72. J. Y. Bottero, J. M. Cases, F. Fiessinger and J. E. Poirier, J. Phys. Chem., **84**, 2933 (1980).

73. J. W. Akitt and A. Farthing, J. Magn. Reson., **32**, 245 (1978).

74. J. W. Akitt and B. E. Mann, J. Magn. Reson., **44**, 584 (1981).

75. J. W. Akitt and A. Farthing, J. Chem. Soc. Dalton Trans., 1606 (1981).

76. J. W. Akitt and A. Farthing and O. W. Howarth, J. Chem. Soc. Dalton Trans., 1609 (1981).

77. J. W. Akitt and A. Farthing, J. Chem. Soc. Dalton Trans., 1617 (1981).

78. J. W. Akitt and A. Farthing, J. Chem. Soc. Dalton Trans., 1624 (1981).

79. J. W. Akitt and W. Gessner, J. Chem. Soc. Dalton Trans., 147 (1984).

80. D. Muller, D. Hoebbel and W. Gessner, Chem. Phys. Lett., **84**, 25 (1981).

81. D. Muller, W. Gessner, H. -J. Behrens, and G. Scheler, Chem. Phys. Lett., **79**, 59 (1981).

82. M. C. Cruickshank, L. S. D. Glasser, S. A. I. Barri and J. F. Poplett, J. Chem. Soc., Chem. Commun., 23 (1986).

83. M. C. Cruickshank, and L. S. D. Glasser, J. Chem. Soc., Chem. Commun., 84 (1985).

84. J-P. Gilson, G. C. Edwards, A. W. Peters, K. Rajagopalan, R. F. Wormsbecher, T. G. Roberie and M. P. Shatlock, J. Chem. Soc., Chem. Commun., 91 (1987).

85. D. Freude and H. -J. Behrens, Cryst. Res. Technol., **16**, K36 (1981).

86. C. A. Fyfe, G. C. Gobbi, J. S. Hartman, J. Klinowski and J. M. Thomas, J. Phys. Chem., **86**, 1247 (1982).

87. J. Klinowski, M. W. Anderson and J. M. Thomas, J. Chem. Soc. Chem. Commun., 525 (1983).

88. C. A. Fyfe, G. C. Gobbi, J. Klinowski, J. M. Thomas and S. Ramdas, Nature (London), **296**, 530 (1982).

89. G. Engelhardt and D. Michel, "High-Resolution Solid-State NMR of Silicates and Zeolites"; John Wiley & Sons: New York, 1987.

90. I. J. Lowe, Phys. Rev. Letters, **22**, 133 (1966).

91. E. R. Andrew, Int. Rev. Phys. Chem., **1**, 195 (1981).

92. A. Abragam, "Principles of Nuclear Magnetism"; Oxford Univ. Press: Clarendon, 1961.

93. E. Kundla, A. Samoson and E. Lippmaa, Chem. Phys. Lett., **83**, 229 (1981).

94. A. Samoson, E. Kundla and E. Lippmaa, J. Magn. Reson., **49**, 350 (1982).

95. A. P. M. Kentgens, K. F. M. G. J. Scolle and W. S. Veeman, J. Phys. Chem., **87**, 4357 (1983).

96. J. W. Beams, Rev. Sci. Instr., **1**, 667 (1930).

97. J. W. Beams, J. Appl. Phys., **8**, 795 (1937).

98. P. A. S. Van Dijk, W. Schut, J. W. M. Van Os, E. M. Menger and W. S. Veeman, J. Phys. E. Sci. Instr., **13**, 1309 (1980).

99. R. A. Wind, F. E. Anthonio, M. J. Duijvestijn, J. Smidt, J. Trommel, and G. M. C. de Vette, J. Magn. Resonance, **52**, 424 (1983).

100. B. C. Gerstein, C. Chow, R. G. Pembleton, and R. C. Wilson, J. Phys. Chem., **81**, No. 6, 565 (1977)

101. D. R. Corbin, B. F. Burgess, Jr., A. J. Vega, and R. D. Farlee, Anal. Chem., **59**, 2722 (1987).

PART TWO. NMR STUDIES OF AMORPHOUS SILICON

INTRODUCTION

Many amorphous solids, for example, ceramics and glass, have been industrially produced and widely used in daily life for hundreds years. It was recently found that amorphous Si and its alloys are very promising material in the field of electronics and energy conversion technologies. A detailed knowledge in structure of these materials is needed to better understand their properties and will lead to the improvement of them. As such, amorphous solids have been extensively studied using a variety of techniques such as X-ray Absorption, X-ray Radial Distribution Function, Laser Raman spectroscopy, Electron Spin Resonance, and Nuclear Magnetic Resonance. An enormous effort has been made to investigate its technologically useful properties which are sharp functions of the micro-structure of the material. Progress in the central problem of amorphous Si, the determination of its structure at the atomic level, has been slow and is one of the least understood areas of all of theoretical physics.

LITERATURE REVIEW

The early work on a-Si and a-Ge concentrated on two areas. First was the measurement of the physical properties such as the long wavelength index of refraction, the density and the conductivity. Second was to find a model system.

Before 1970, the characterization of the physical properties of amorphous Si and Ge was ill defined, with markedly different values having been published. In 1971, the publication of systematic studies of the variation of physical properties with deposition conditions and annealing changed this situation. It was found that the physical properties of amorphous materials are strongly dependent on the deposition conditions. Experimental evidence implies that the physical properties of amorphous materials are related to the range of the so-called local order or short-range order which in turn depends on the material and the conditions of formation of the amorphous solid.

In 1932, Zachariasen[1] suggested an idealized model for the structure of covalently bonded amorphous solids. He showed a two-dimensional graph representing an amorphous binary compound of A_2B_3. In this structure, each A atom is covalently bonded to three B neighbor atoms in an approximately triangular arrangement and each B atom is covalently bonded to two A neighbor atoms. Variations in bond

angles, not permitted in the crystal, causes the lack of long range order. It is this model that has led to the concept of the continuous random network (CRN model) widely used for theoretical work on amorphous material.

Information about short-range order in amorphous solids is usually obtained from diffraction measurements. In 1969, Moss and Graczyk[2] obtained the experimental radial distribution function (RDF) of a-Si from X-ray diffraction. The RDF is a measure of the probability of finding two atoms at a distance, r, from each other in the material. The relatively sharp peak of the first-neighbors which represents the distribution function of bond length indicates a small deviation in bond length. The peak of the second-neighbor is broad and overlaps with the peak of the third-neighbor due to both deviations in bond length and bond angle. Unlike the RDF of crystal Si, no further peaks can be seen. The RDF clearly shows the presence of short-range order and the lack of long-range order in amorphous materials. But Moss and Graczyk found no model which gave a possible fit. The random-network structure suggested by Zachariasen was quite rough so that it cannot correctly predict the RDF.

In the last two decades numerous different groups have undertaken the building of models for amorphous materials. Due to its simple chemical bonding and composition, tetrahedrally coordinated amorphous Si and Ge are ideal prototypes for the study of the disordered systems.

The microcrystalline models[3] are heterogeneous in that the microcrystals are separated from each other by a disordered boundary

region of connective material. Correlations between atomic positions are very high at small separations, and then decrease abruptly when the separation traverses a boundary. G. Etherington et al.[4] studied RDFs of amorphous Si by neutron diffraction techniques and compared the results with various structural models. They found that the structure of amorphous materials with tetrahedrally coordinated atoms is not adequately described by microcrystalline models based on the diamond, Wurtzite, Si III and Ge III polymorphs and that a better fit is obtained for CRN models. The microcrystalline model cannot generate a first peak as sharp as the one from experiments without also yielding too-sharp peaks at large separations.

In 1973, Polk and Boudreaux[5] constructed a hand-built model for tetrahedrally bonded amorphous materials based on Zachariasen's concepts. In this structure, each atom is fourfold coordinated in an approximately tetrahedral arrangement. Bond lengths are constant. Variations in the tetrahedral angle and the relative rotation of adjoining tetrahedra into configurations other than the staggered or eclipsed configurations found in the diamond cubic and wurtzite structures results in the lack of long range order. Polk recognized that because the coordinates of the atomic positions in the structure were not obtained, the properties of the structure such as its diffraction behavior, electronic energy levels, and vibrational spectra could not be calculated. Further, statistical data for the structure were incomplete and difficult to obtain. He determined the atomic coordinates of the random network structure model and refined the first-neighbor distance using computer aided fitting so that the

standard deviation of the first-neighbor distance was less than a predetermined value. The RDF calculated from the model agrees well with the experimental result. There are a relatively sharp first peak and a broad second peak in the expected locations. No peak appears in the vicinity of the crystalline third-neighbor distance. Beyond the third-neighbor distance, the subsequent peak heights rapidly converge to the average-density line, the parabola.

Henderson and Herman[6] constructed a CRN model by computer with periodic boundary conditions and 64 atoms in the unit cube. The atoms were initially positioned on a diamond lattice and randomly displaced. the atomic coordinates were then systematically adjusted to minimize the spread in nearest neighbor separations. Due to a large distortion in local tetrahedral bonding, the resulting model exhibits bond angle distortions which appear to be unrealistic. The positions of the first and second peaks, their respective areas and the mean bond angle of 109.2° indicate that the basic structural unit is the tetrahedron. Above 5 Å the RDF calculated from the model exhibits much less structure than found experimentally, showing that in the model there is very little correlation between the positions of third and subsequent neighbors.

Evans et al.[7,8] obtained a CRN model via a decoration transformation[9] of the vitreous SiO_2 random network model of Evans and King[10]. This involved removing the oxygen atoms and regularising the resulting network to give a first neighbor distance distribution appropriate to amorphous Si. The model accurately predicts the first two peaks and also the general characteristics at

larger separations. The disagreement between Evans' model and experiment are significant differences between 4.5 Å and 5.5 Å, a range dominated by third neighbor interactions, and the RDF of the model also exhibits too much structure at higher separations.

The RDF of various CRN models were compared with the experimental RDF by Etherington et al.[4] It is concluded that all the above three models reproduce the main features of the experimental RDF, but of the three the Polk model gives the best fit. They noticed that although it is difficult to associate ring statistics with detailed features in the RDF, the four models which provide the best fit to experiment (i.e., due to Beeman and Bobbs[11], Steinhardt et al.[12, 13], Boudreaux et al.[14], Duffy et al.[15] and Polk and Boudreaux[5]) all have ring statistics falling within the same approximate range. It is found for these models that 6-membered rings are most probable, followed in order of preference by 5-membered, 7-membered and 8-membered rings.

Because many of the characteristic properties of a-Si depend crucially on short range order[16] and most attempts to interrupt the main features of the RDF of a-Si have relied on structural models, devoting of a large effort to the attempt to construct structure models of a-Si has been continued. Since then Polk's model was refined by many workers and impressive agreement with experiments was obtained.

The generally accepted idea about a-Si, within the CRN model are as follows:[17]

(1) z=4, each atom is fourfold coordinated.

(2) Constant bond lengths.

(3) No dangling bonds.

(4) There is a significant spread in bond angle.

(5) There is no long-range order.

This simple model implies that the bond length variation is zero, as in the crystal. Unlike the crystal, the Si-Si-Si bond angle takes on a distribution which results in the lack of long range order in the a-Si.

Wooden and Weaire suggested that the required characteristics of model building were:[18]

(1) The model should contain at least several hundred atoms.

(2) The model should conform to periodic boundary conditions.

(3) the distortion of local tetrahedral bonding should be limited in a range small enough.

The periodic boundary conditions enable surface effects to be avoided and long range interactions to be included in an elementary way and are desirable when pseudopotential methods are used in electronic structure calculations. But the periodic boundary conditions also have the effect of introduction of pseudo-crystallinity. Hence the model must be large enough to avoid this problem.

Winer further suggested that the models should be computer-generated to eliminate the bias that can occur in hand-built models and the RDF of the models should show no serious discrepancy when compared

to experiment[19] with these guidelines and computer aided calculations.

They developed a random-network model of a-Si with periodic boundary conditions.[20] The model contained 216 atoms. Model construction began with the diamond cubic structure. After each bond rearrangement, the structure was partially relaxed by use of the Keating potential,[18,21] with a bond-bending to bond-stretching ratio of $\beta/\alpha=0.285$. Not only are the calculated RDF and geometric distortions of the model in good agreement with experiment, but also the phonon density of state, Raman and IR spectra compare well with experiment

In addition to above conventional ball and stick models, Car and Parrinello[22] obtained an a-Si structure with a computer simulation based on a new first-principles molecular dynamics scheme[23] in which the interatomic potential is constructed directly from the electronic ground state and is treated with accurate density-functional techniques used in electronic-structure calculations.[24] Both calculated RDF and vibrational spectrum of a-Si agree very well with the experiments. The relative strength of the TA and TO peaks in the vibrational spectrum is similar to that of experiment while all other model calculations give a larger amplitude to the TO peak.[19,25]

In addition to RDF, Raman and inelastic neutron scattering study also provided significant data. Maley et al.[26] compared the neutron G(E) spectra of a-Ge and c-Ge. He found that the primary changes with structural order occur in the TO band which has a more intense, narrower peak for the c-Si. This behavior parallels the results of

theoretical G(E) calculations.[27,28] Similar behavior for the form of G(E) in a-Si has also been observed.[29] As the TO band width, Δ, is approximately proportional to the width of the bond angle distribution,[30] the narrower TO peak indicates the narrower distribution of bond angle in a-Si. The bond angle distributions is found to be Gaussian, and the deviation is estimated as approximately 9° to 11°. Fortner and Lannin[31] performed both neutron diffraction and Raman scattering measurements on two forms of amorphous Si prepared by low pressure RF sputtering and by subsequent annealing at 600 °C. He compared the two RDFs. The position of the first peak in the RDFs is unchanged. Only very small changes of about 0.1% were observed in its width after correcting for thermal broadening. The positions of the lower portion of the second peak in RDFs indicate that the most probable values of the tetrahedral angle for as-deposited and annealed films are 108.4° and 108.6°, respectively, versus 109.5° in crystalline Si. The form of the lower part of the second RDF peak indicated substantial changes in width that reflects short range order variations in the bond angle distribution. This yields a change of 11% in width of bond angle distribution after the a-Si sample was annealed at 600 °C. measurements of the high frequency band designated as the TO band, shows that annealing at 600 °C reduces this band width from 109 cm^{-1} to 87 cm^{-1}.

EXPERIMENTAL

The a-Si samples studied in the present work were prepared in the research group of Professor Jeff Lannin of Pennsylvania State University and Joseph Shinar of Iowa State University. The samples were sputtered from a 12.8 cm diameter target, at 10 m Torr argon pressure, with a 5 cm separation between target and substrate.

A series of measurements on the same amorphous Si sample were taken before and after isochronal anneals at increasing temperatures from 400 °C to 640 °C in order to ensure significant comparison between the different results. The measurements included X-ray diffraction, electron spin resonance and MAS NMR.

To anneal the a-Si sample, the amorphous Si sample was sealed in a 7 mm quartz tube under vacuum, the quartz tube was kept at anneal temperature for one hour, and was then cooled to room temperature over a period of 10 minutes. The isochronic annealing temperature was between 400 and 640 °C with steps of 30 °C. After each anneal the sample was removed from the quartz tube for the measurements.

The ESR signals were measured at room temperature in X-band on a Bruker ESR spectrometer. The absolute number of spins was not obtained due to the lack of a calibrated standard sample. The relative values of spin density were found by comparing the signals of the sample with those of a stable uncalibrated Picein 80 standard sample. The accuracy

of comparison was estimated to be about ±10%, limited by the reproducibility of insertions and cavity tuning. Each comparison was repeated, and results presented were averages of all comparisons for a given annealing condition. The g factor of the signal was determined from a comparison with a standard DPPH sample

The X-ray diffraction pattern of the a-Si were performed in a Scintag Pad V spectrometer using copper Kα radiation incident at a glancing angle.

The ^{29}Si MAS NMR spectra were taken at 43.72 MHz on a home-build spectrometer (see Part I). The sample spinning speed is about 5.0-5.2 KHz. A dwell time of 2 microseconds was used for all measurement with annealing temperature below 640 °C. After 640 °C annealing the dwell time was 20 microseconds to provide added resolution for observation of the narrowed a-Si peak. After each step of annealing the longitudinal relaxation time, T_1, of the sample was measured first and then the experiment recycle time was set to be longer than $5T_1$. Ninety degree pulse, 2K data points, 4K Fourier transform, 10 KHz audio filter and quadrature detector were used in all experiments.

RESULTS AND DISCUSSION

Figures 1, 2, 3 and 4 show the powder X-ray diffraction intensity plots for the amorphous Si samples at three representative stages in a series of isochronal anneals. Figure 1 is the spectrum before annealing. Figure 2 is typical of the pattern after each of six isochronal annealing steps, and was taken after the sample was annealed at 580 °C. Figure 3 was taken after the sample was annealed at 610 °C. Figure 4 was obtained after a subsequent anneal at 640 °C. The main feature of these X-ray diffraction pictures are as follows:

(1) All patterns of amorphous Si under 580 °C are essentially the same. There is no sharp peak. This indicates that there is no long range order in the material. There is only a broad peak at about angle of 28°. In crystalline Si the peak at 28.4° corresponds to the Bragg reflections from (111) planes.

(2) The patterns for all annealing temperatures above 610 °C are similar. Three sharp peaks appear at 28.6°, 47.5° and 56.5°, respectively, (see Figure 5). These peaks are characteristic of fine-grain polycrystalline Si. The intensities of these peaks increase with the annealing temperature. This result indicates that the crystallization of amorphous Si first becomes observable in the range of 580-610 °C

(3) After annealing at 520 °C, an unknown peak appears at 38.5°. Although its intensity is low, it remains present until after annealing at 640 °C. No known c-Si structure matches with this peak at 38.5°. Two more a-Si samples were prepared, treated and measured under same conditions until annealing at 580 °C. No peak was observed at 38.5°. Also there is no peak at 38.5° in the background spectrum. The NMR spectra in the temperature range from 510 to 610 °C did not show additional peaks.

The ESR signal of amorphous Si was strong and easy to detect at room temperature. Figure 6 shows the variation of the relative spin density of the sample with annealing temperature. At all observation temperatures the g value of the resonance is 2.0055±0.0005. The line shape is basically Gaussian.

The MAS NMR spectra are shown in Figures 7-9. Figure 7 is typical of the pattern after each of seven isochronal annealing steps, and was taken after the sample was annealed at 580 °C. The NMR spectra of amorphous Si for all annealing temperatures below 580 °C are essentially the same. Only a single peak with about 80 ppm of FWHM is present. The X-ray spectra of these samples showed no sharp peaks. These results indicate that only an amorphous phase exists in the sample in this temperature range. The peak is nearly symmetric. The first moment of the peaks varies slightly with annealing temperature from -38 ppm without annealing to -43 ppm after annealing at 580 °C. The second moments decrease with the annealing temperatures from 1183 ppm^2 to 823 ppm^2. After annealing at 610 °C a sharp peak with a FWHM of about 10 ppm appears at about -78 ppm. Figure 8 shows the spectrum.

The first moment of the spectrum is -62 ppm. The chemical shift of the narrow peak is the same as that of crystal Si. Also, for the sample annealed in this temperature range, the characteristic peaks of c-Si appeared in the X-ray spectrum. This indicates both amorphous and crystalline Si phases were present in the amorphous Si sample after anneal at 610 °C. The intensity of the narrow peak representing crystal Si in the sample increases when the recycle time of NMR experiments increases from 320 seconds to 600 seconds while the intensity of the broad peak did not change. It indicates that the longitudinal relaxation time T_1 of the sharp peak is much longer than that of the broad peak, and longitudinal relaxation in crystalline Si is much slower than that in a-Si phase. The first moment of the broad peak representing the a-Si phase in the sample is -58 ppm and its second moment is 810 ppm^2. The T_1 of amorphous Si was found to be about 80 seconds, similar to that of the sample after annealing at 580 °C, which is about 71 seconds. The T_1 of crystalline Si is about 200 seconds. Figure 9 shows the spectrum taken after the sample was annealed at 640 °C. In Figure 9 the broad peak has disappeared. The only peak present in this spectrum appears at -78 ppm with FWHM of 7 ppm. Compared to the spectrum of crystalline Si, which is at -78 ppm and with a width of less that 0.3 ppm, this peak is inferred to represent crystalline Si with residual disorder still present. Figure 10 shows the variation of T_1 with temperature.

Both c-Si and a-Si are solids. The Si nuclei is spin 1/2. The only broadening interactions present are the homonuclear dipolar interaction and the shielding anisotropy (zero for Td symmetry) which

are removed under fast magic angle spinning. For a solid elemental sample such as c-Si or a-Si, the chemical shift of each atom is determined by the local structure of the atom and can be seen as a cerwtain function of the parameters of its local structure, for example bond length, bond angle, the number of nearest neighbors and so on. In crystalline Si the arrangement of all Si atoms are highly ordered. Any Si atom and its local structure can be used as being representative of all others. All Si atoms in a sample of perfectly crystalline silicon have exactly the same environment and the same chemical shift. The MAS NMR spectrum of crystalline Si taken on our NMR spectrometer shows a line at -78 ppm with a FWHM of less than 0.3 ppm. The line width in this case is mainly due to the inhomogeneity of the static magnetic field. On the other hand, in an a-Si sample the distributions in the local structural parameters such as bond angle, bond length, and dihedral angle dictate that the local structure of all atoms in the sample are described by a distribution of environments. The distributions in parameters of local structure cause a distribution in chemical shift of the Si atom. The broadened peak observed in MAS NMR spectrum of amorphous Si is an inhomogeneously broadened envelope of all these peaks and represents the distribution in chemical shift of all Si atoms.

Lannin[32] indicated that it is necessary to involve statistical methods to specify the local structure of a-Si. One must describe the distribution of nearest neighbors in distance, number and angles about an atom. Some statistical data of local structure can be obtained from various experiments. For example, the first peak of the RDF actually

is the distribution function of bond length. The location of its highest point is the most probable value of bond length. For a symmetric peak it is also the average value of bond length. The area under the peak represents the average number of nearest neighbors. From the peak width the standard deviation of the distribution of bond length can be calculated. It can be assumed that every structural parameter has a distribution and there is a most probable value, the location of the highest point of the distribution, an average value, and a standard deviation for this parameter. A local structure is called the most probable local structure if its all structure parameters have their most probable values. The chance to find a Si atom with the most probable local structure in the a-Si sample is highest. As a result the Si atoms with the most probable local structure give the strongest signal in a NMR spectrum of a-Si. The NMR spectrum of a-Si shows the distribution of chemical shifts of Si atoms in the amorphous sample. It also has a most probable value. As a function of all parameters of local structure, the most probable value of chemical shift corresponds to the Si atoms with the most probable local structure in the a-Si sample.

The fact that the X-ray spectrum taken after annealing at 640 °C shows the three characteristic lines of powdered c-Si (see Figure 5) indicates that the sample is characterized by a high degree of crystallinity. The MAS NMR spectrum of this sample also shows that only one peak at -78 ppm, characterizing the chemical shift of c-Si, is present in the spectrum. The broad peak centered at about -50 ppm has disappeared. Compared to c-Si, both the X-ray spectrum and the MAS NMR

spectrum of this sample are broadened. The peak width of 7 ppm, which is much greater than the value of 0.3 ppm observed for c-Si, and much less than 80 ppm observed for a-Si, shows an narrowed distribution in chemical shift and indicates a much narrower distribution in the local structural parameters of Si atoms in the sample. Only residual disorder exists in the sample. The maximum is at -78 ppm corresponding to the most probable local structure in the sample. The coincidence of this most probable value with the chemical shift of c-Si implies that the most probable local structure of this sample is same as the structure of c-Si. These results indicate that long range order has been established in the sample, and that the primary local structure is that of c-Si. Yet a small variation from the structure of c-Si in local structure, most probably in bond angle remains, resulting in a distribution in chemical shift larger than broadening due to d.c. field inhomogeneity.

There are two peaks in the MAS NMR spectrum of a-Si after annealing at 610 °C. Both seem nearly symmetric. One narrow peak is at -78 ppm and another broad one is at -53 ppm. The narrow peak at -78 ppm is similar to that in spectrum taken after annealing at 640 °C. It is taken to represent the crystalline phase in the sample. The most probable local structure of Si in the phase is the same as that of c-Si. The broad peak representing the amorphous portion of the sample shows a different distribution of chemical shifts not only in peak width but also in peak location. The width of 80 ppm indicates a much more severe disorder present than in crystalline phase. The locations of the highest points, the most probable chemical shift, of the two

peaks do not coincide with each other. The substantial difference of more than 30 ppm in location between the two peaks indicates that the most probable local structures of the two phases are not the same. This means that the structure of c-Si is not the most probable local structure of the a-Si phase. At least one of the most probable values of local structure of the sample, e.g., bond length, bond angle, dihedral angle or ring size, perhaps more, is not the value found in c-Si. This difference in the most probable local structures of the two phases causes the 30 ppm difference in chemical shift. The dangling bond susceptibility cannot cause an effect of this magnitude. See below. It may also be inferred that in an a-Si sample only small fraction of Si atoms have a local structure similar to that of c-Si. Fortner's RDF studies indicated that the most probable values of tetrahedral angle for as-deposited and annealed a-Si films are 108.4° and 108.6°, respectively, instead of 109.5° in c-Si.

Only one broad peak representing a-Si appears. The differences between these spectra are the variations of first and second moment with annealing temperature. The structure of a-Si is thermodynamically unstable with respect to c-Si. Under annealing the Si atoms in a-Si tend to rearrange toward the thermodynamically stable structure, that of c-Si. Thermal relaxation in the a-Si sample will increase the local order. The local structural parameters in a-Si will tend to approach the corresponding values found in c-Si, and distributions of these parameters will reduce to zero or near zero, which is the distribution in c-Si. The results are that the first moment of the NMR spectrum, the average chemical shift of all a-Si atoms in the sample, moves

towards -78 ppm, the chemical shift value of c-Si. The second moment, the mean square deviation of chemical shift distribution, reduces with increasing of annealing temperature. Figure 11 shows that under 610 °C the first moment of the NMR spectra varies slightly with annealing temperature. The variation is from -38 ppm to -41 ppm after annealing at 400 °C and from -41 ppm to -43 ppm with increasing annealing temperature until 580 °C. The first moment is -55.7 ppm after annealing at 610 °C and -81 ppm after annealing at 640 °C. Figure 12 shows the relative second moment, which is $M_2(t)/M_2(t=20°C)$, versus annealing temperature. This value decreases under 640 °C from 360 ppm^2 to 280 ppm^2. There is a steep drop from 280 ppm^2 to 29 ppm^2 due to the completion of crystallization of a-Si after annealing at 640 °C. The negative slopes in both Figure 11 and 12 before annealing at 640 °C indicate that short range order was increased after each step of anneal. Both steep drops in the two figures after annealing at 640 °C indicate the completion of crystallization. The very slow variation of the first moment with annealing temperature until 580 °C implies that the average values or the most probable values of local structure of the a-Si sample changes little in this annealing temperature range. The main variation is the reduction of width in distributions of structural parameters, associated with a reduction in width of distribution of the chemical shift.

The existence of dangling bonds may cause an additional chemical shift of nearby Si atoms. This additional chemical shift is proportional to the absolute value of spin density. Although the absolute value of spin density was not obtained from the ESR

measurements, it can be seen that at least the spin density of the a-Si sample is not the main reason that results in the 30 ppm difference in chemical shift of a-Si from that of c-Si. The ESR measurements show that the spin density of the sample after annealing at 640 °C is about one tenth of that of the a-Si sample and that the spin density of a-Si varies significantly with annealing temperature. If the spin density of a-Si was the main reason for difference in 30 ppm in the chemical shift of a-Si phase from that of c-Si phase, it would also result in about 3 ppm difference in chemical shift of c-Si phase from that of single c-Si sample in which the spin density is negligible. Also the location of the a-Si peak in MAS NMR spectrum would be expected to vary with the spin density of unpaired electrons. The chemical shift of c-Si phase in the annealed a-Si sample is same as the chemical shift of single c-Si sample within experimental error. The peak location of a-Si does vary slowly with the annealing temperature towards the location of c-Si peak, but it does not scale with changes in the measured electron spin density. As a consequence, the difference of 30 ppm in chemical shift between a-Si and c-Si is inferred to be mainly associated with the difference of local structure.

CONCLUSIONS

This study indicates that:

(1) The crystallization of the a-Si sample approaches an observable rate between 580 °C and 610 °C.

(2) The difference between the chemical shift of c-Si and the first moment of a-Si NMR peak is about 30 ppm. This difference is associated with the differences between the structure of c-Si and the most probable structure of a-Si.

(3) When annealing under 610 °C the local structure of a-Si is modified. The modification of local structure is inferred to be mainly in the reduction of distribution width of the local structure parameter, while average values or most probable values change relatively little.

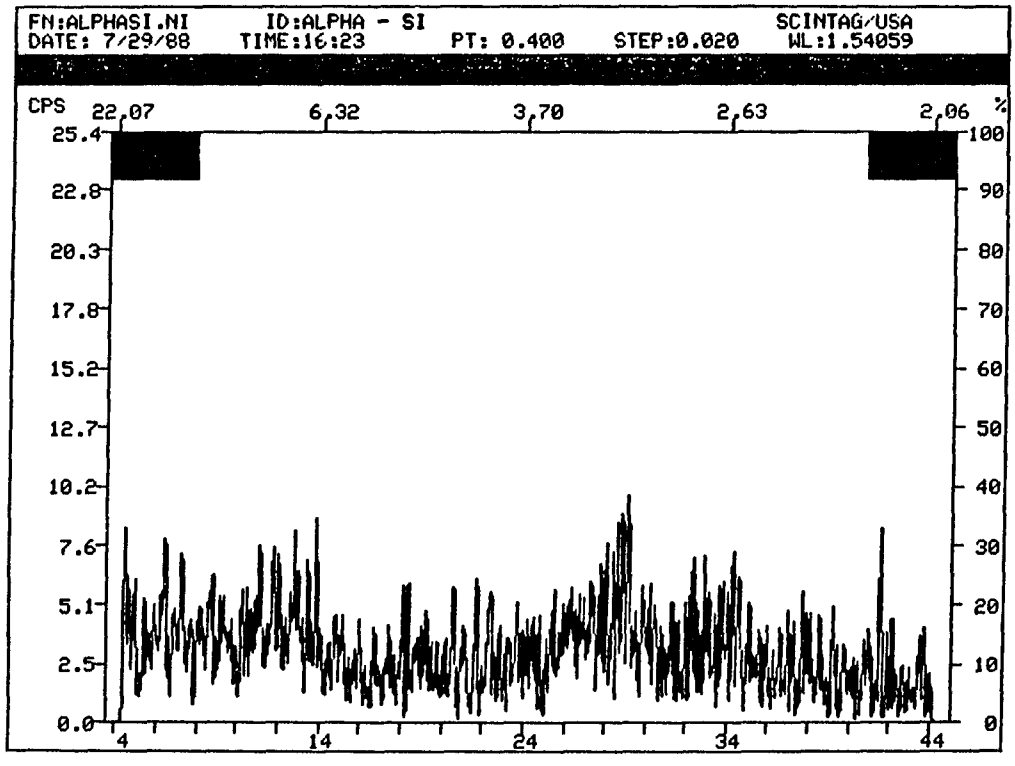

Figure 1. X-ray diffraction pattern of a-Si without annealing

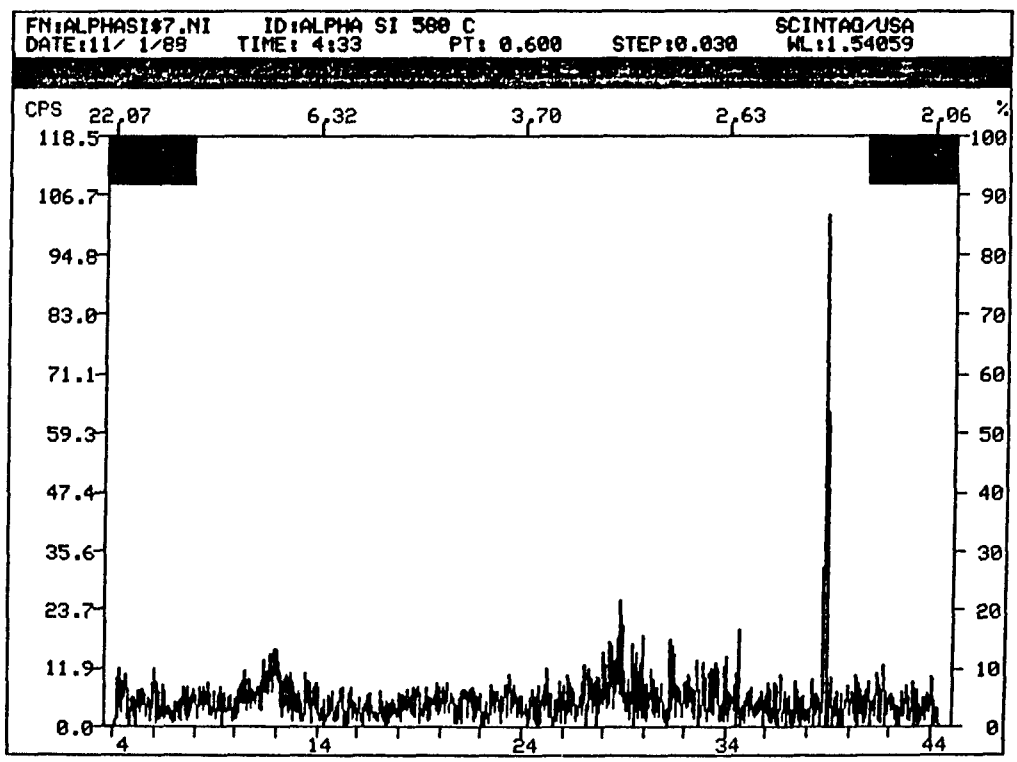

Figure 2. X-ray diffraction pattern of a-Si after annealing at 580 °C

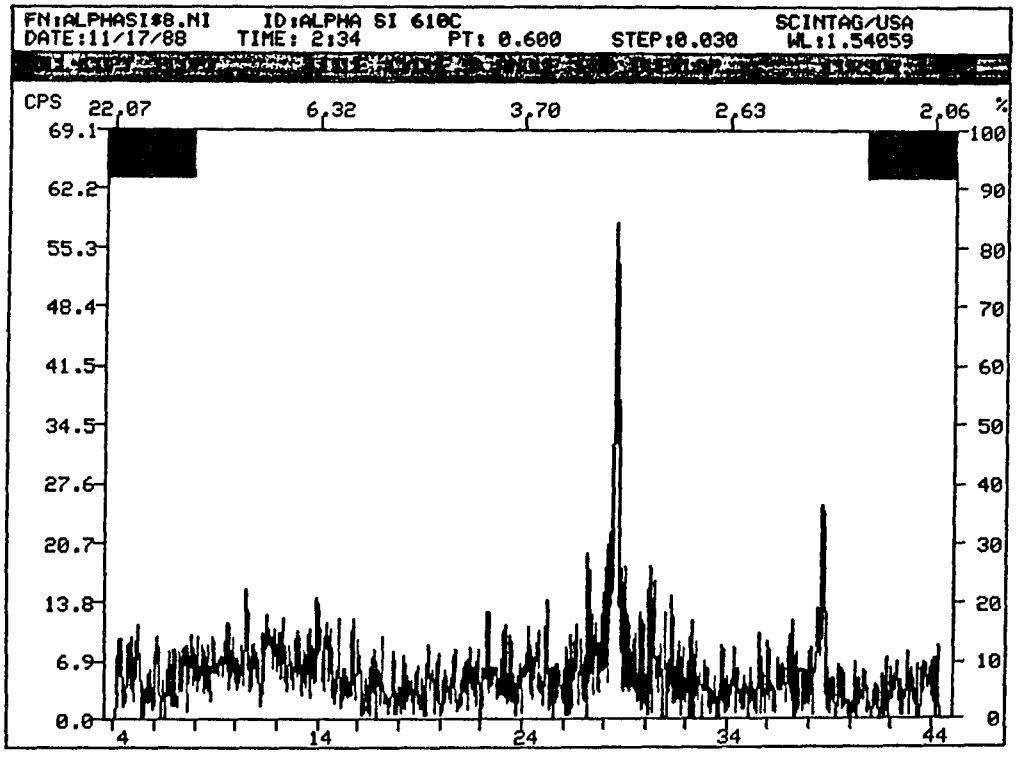

Figure 3. X-ray diffraction pattern of a-Si after annealing at 610 °C

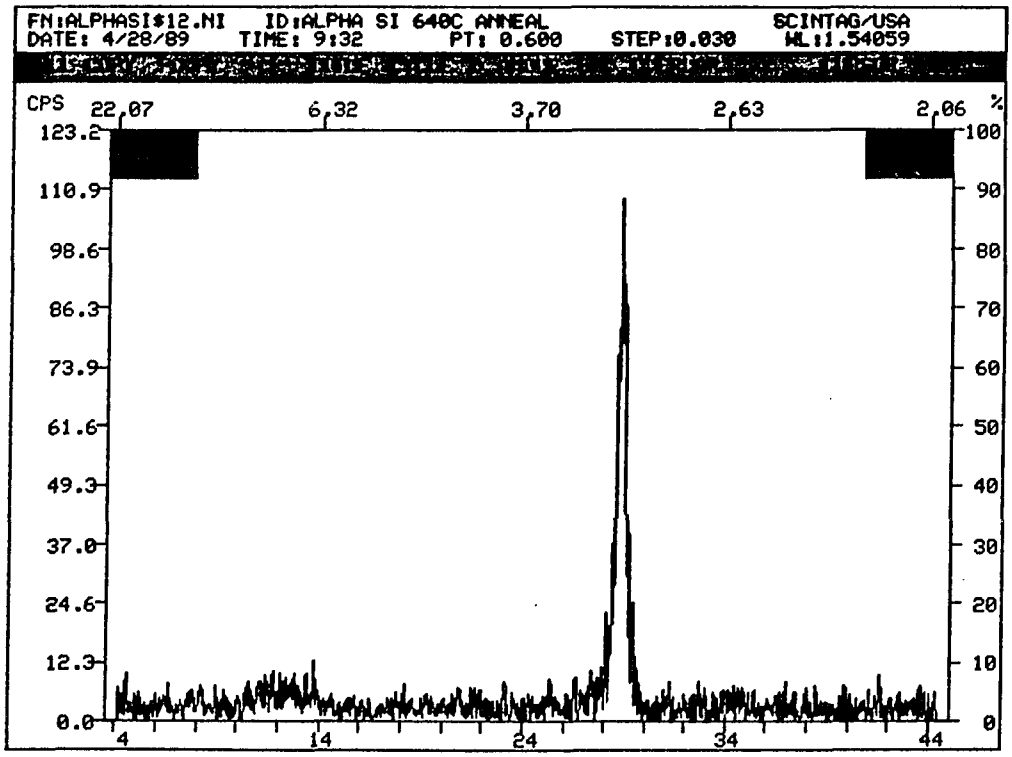

Figure 4. X-ray diffraction pattern of a-Si after annealing at 640 °C

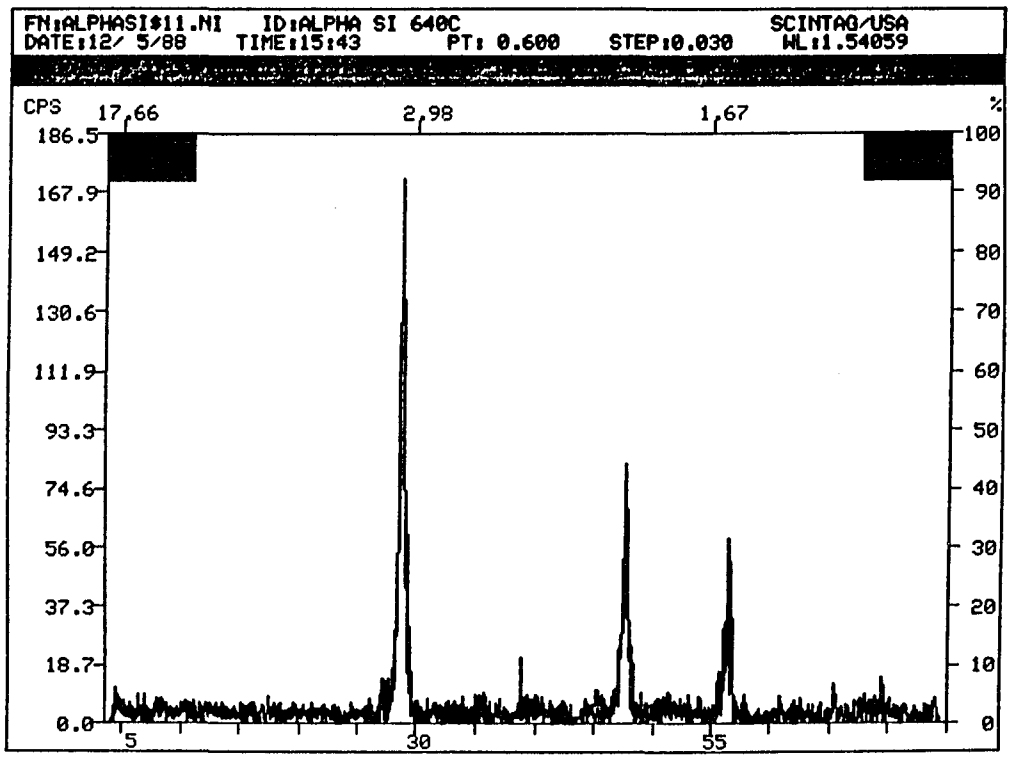

Figure 5. X-ray diffraction pattern of a-Si after annealing at 640 °C

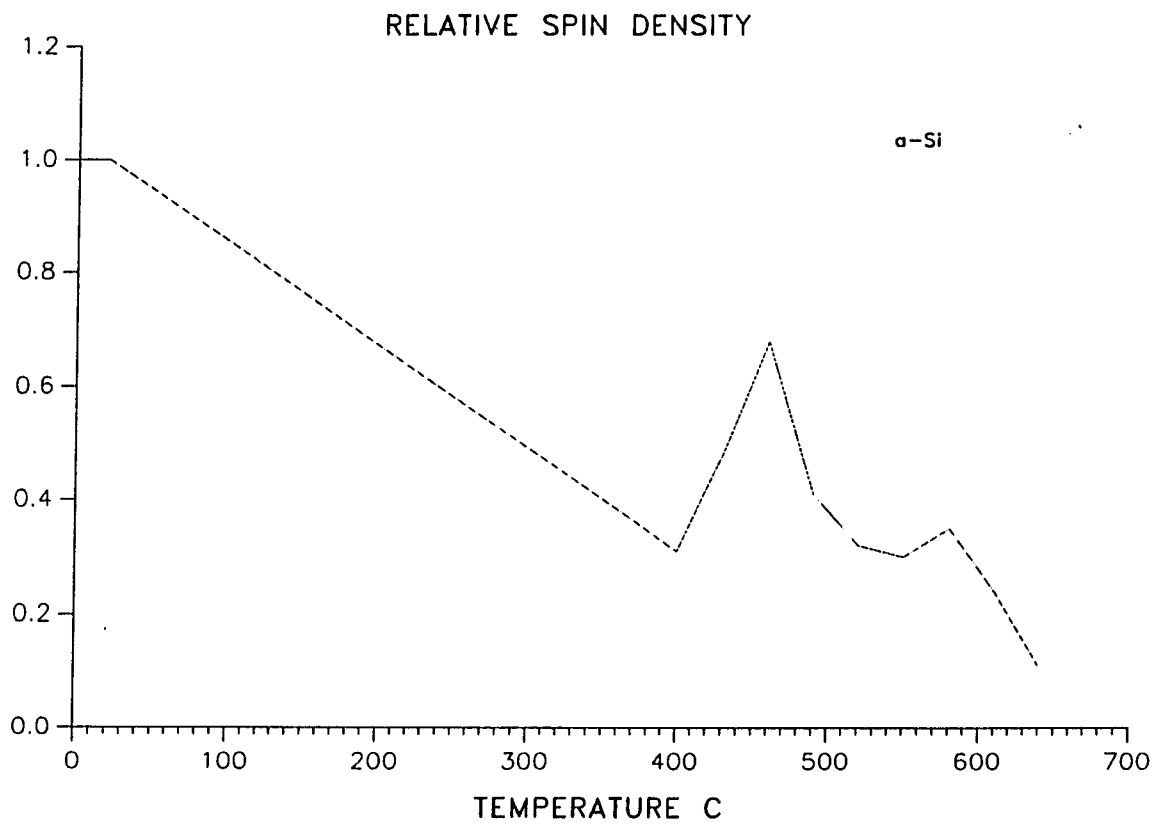

Figure 6. Relative spin density of a-Si vs annealing temperature

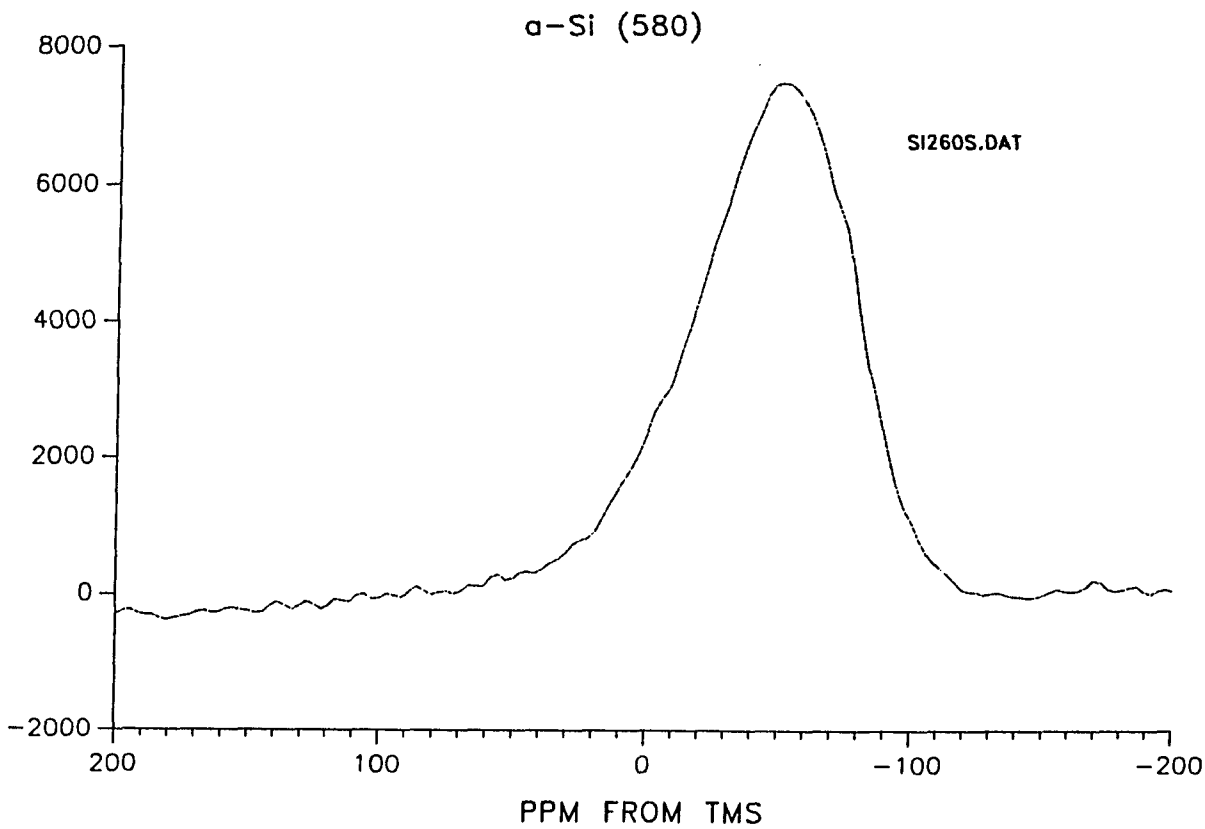

Figure 7. MAS NMR spectrum of a-Si after annealing at 580 °C

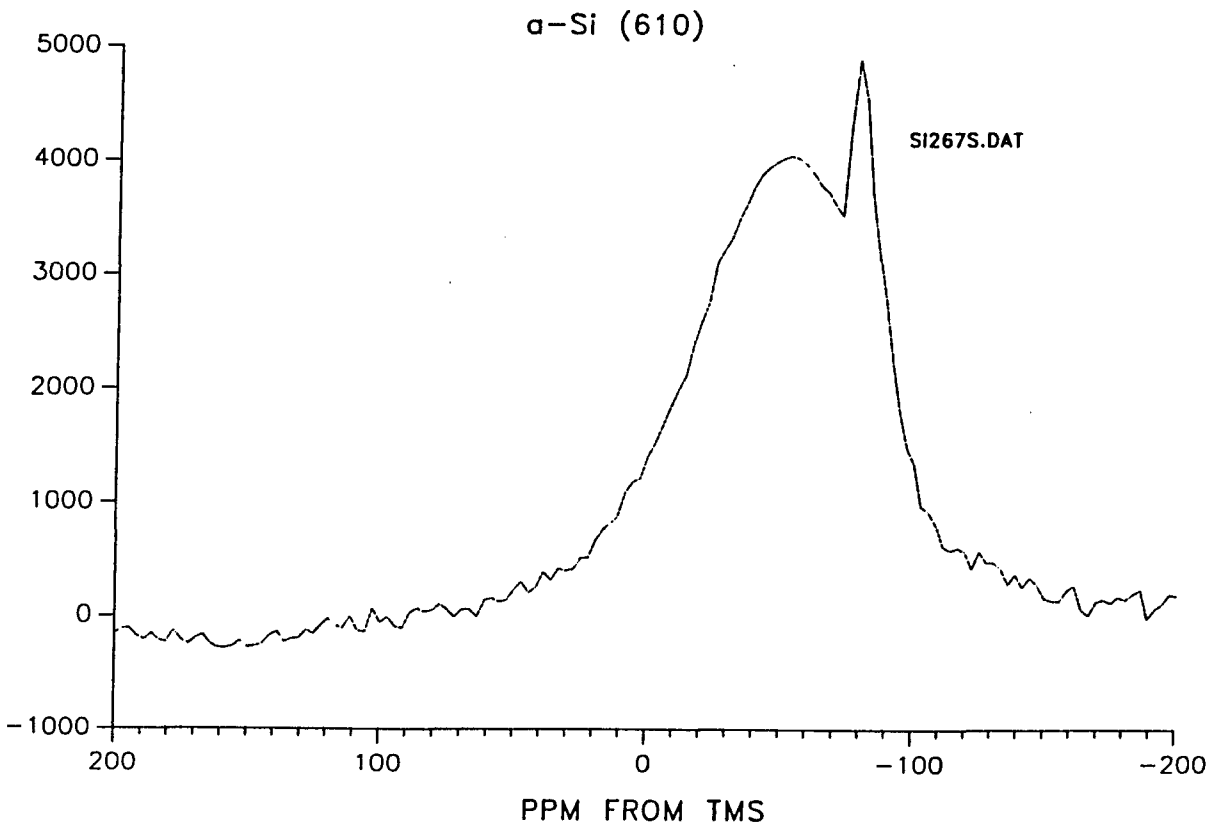

Figure 8. MAS NMR spectrum of a-Si after annealing at 610 °C

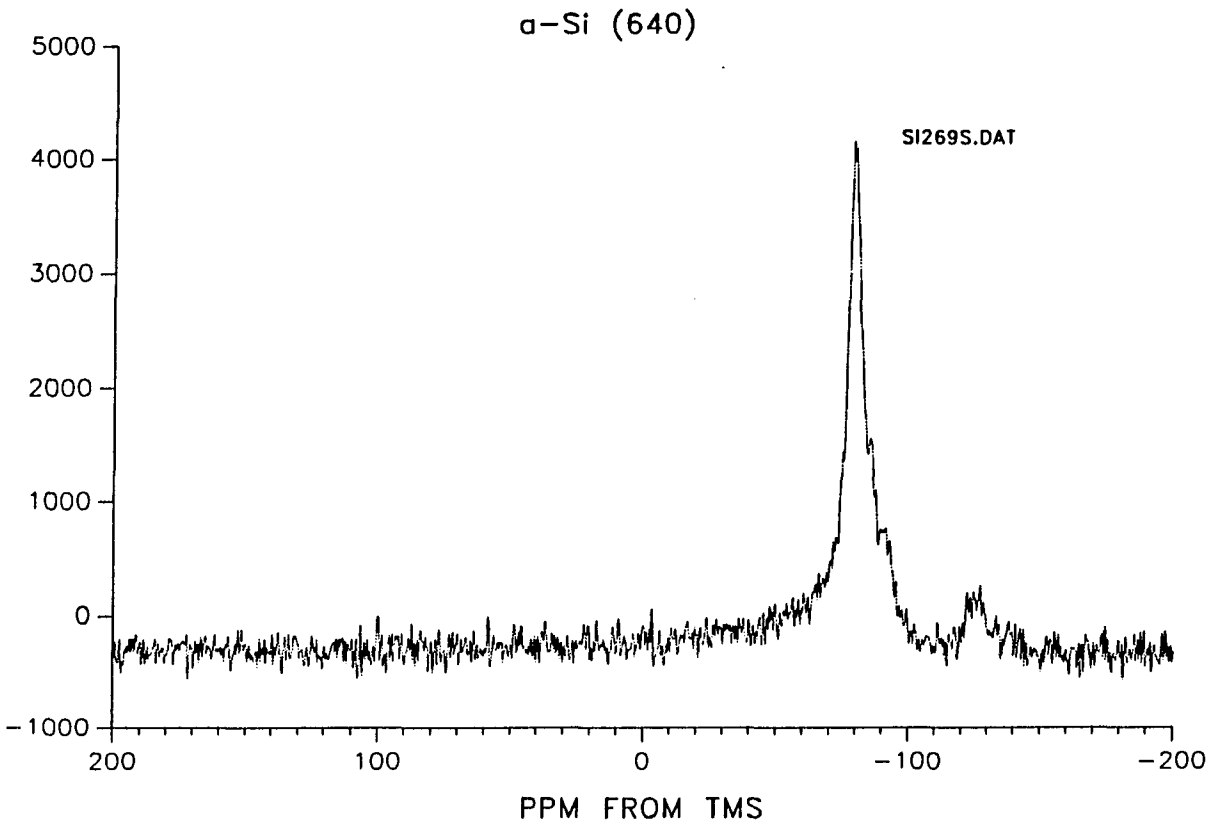

Figure 9. MAS NMR spectrum of a-Si after annealing at 640 °C

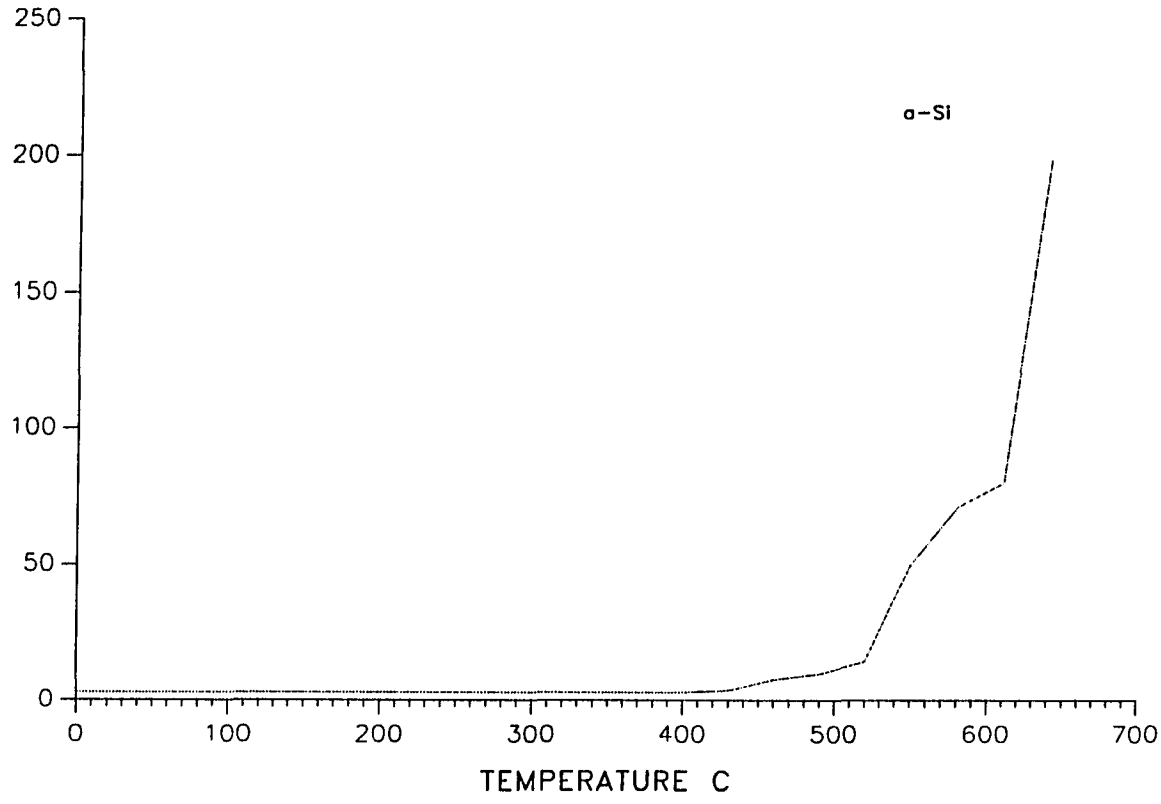

Figure 10. The longitudinal relaxation time of a-Si vs annealing temperature

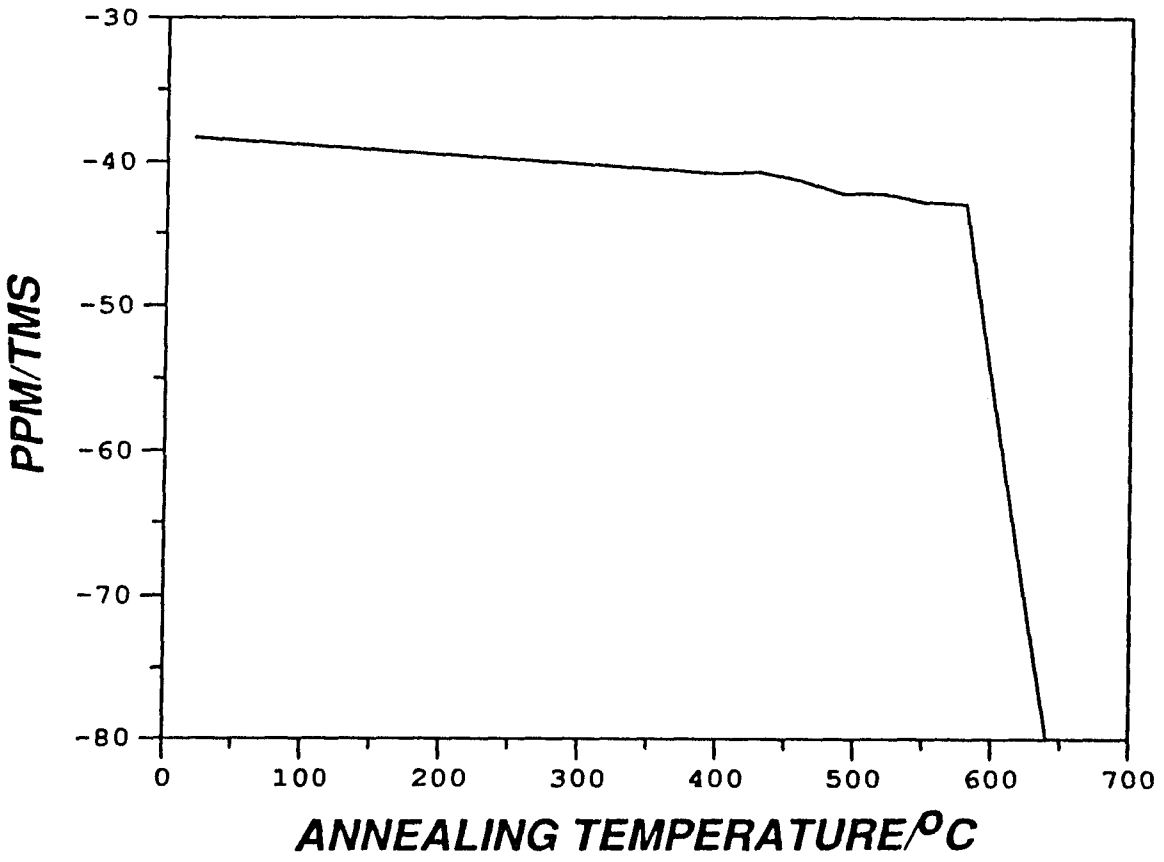

Figure 11. The first moment of NMR spectrum of a-Si vs annealing temperature

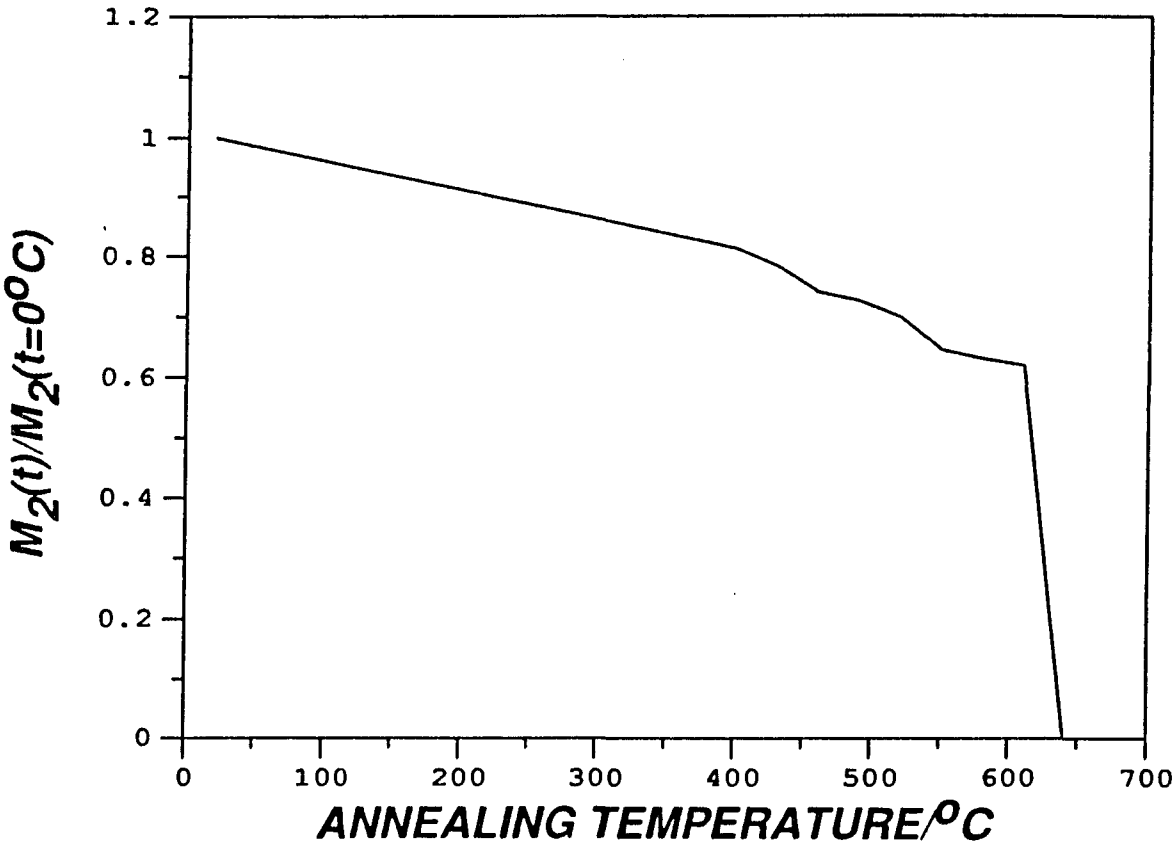

Figure 12. The relative second moment of NMR spectrum of a-Si vs annealing temperature

REFERENCES

1. H. Zachariasen, J. Am. Chem, Soc., **54**, 3841 (1932).

2. S. C. Moss and J. F. Graczyk, Proc. 20th Int. Conf. Phys. Semicond.; USAEC: Springfield, VA, 1970, p. 658.

3. A. J. Leadbetter and A. C. Write, J. Non-Crystallogr. Solids, **7**, 23 (1972).

4. G. Etherington, A. C. Write, J. T. Wenzel, J. C. Dore and J. H. Clarke, J. Non-Crystallogr. Solids, **48**, 265 (1982).

5. D. E. Polk and D. S. Boudreaux, Phys. Rev. Lett., **31**, 92 (1973).

6. D. Henderson and F. Herman, J. Non-Crystallogr. Solids, **8-10**, 359 (1972).

7. D. L. Evans, M. P. Teter and N. F. Borrelli, A. I. P. Conf. Proc., **20**, 192 (1974).

8. D. L. Evans, M. P. Teter and N. F. Borrelli, J. Non-Crystallogr. Solids, **17**, 245 (1975).

9. A. C. Write, G. A. N. Connell and J. W. Allen, J. Non-Crystallogr. Solids, **42**, 69 (1980).

10. D. L. Evans and S. V. King, Nature, **212**, 1353 (1966).

11. D. Beeman and B. L. Bobbs, Phys. Rev. B, **12**, 1399 (1975).

12. R. Alben, P. Steinhardt and D. Weaire, A. I. P. Conf. Proc., **20**, 213 (1974).

13. P. Steinhardt, R. Alben and D. Weaire, J. Non-Crystallogr. Solids, **15**, 199 (1974).

14. D. S. Boudreaux, D. E. Polk and M. G. Duffy, A. I. P. Conf. Proc, **20**, 206 (1974).

15. M. G. Duffy, D. S. Boudreaux and D. E. Polk, J. Non-Crystallogr. Solids, **15**, 435 (1974).

16. W. Paul, G. A. N. Connell, and R. J. Temkin, Adv. Phys., **22**, 529 (1973).

17. R. Zallen, "The Physics of Amorphous Solids"; John-Wiley & Sons: New York, 1983.

18. F. Wooden and D. Weaire, J. Non-Crystallogr. Solids, **64**, 325 (1984).

19. K. Winer, Phys. Rev. B, **35**, 2366 (1987).

20. F. Wooten, K. Winer and D. Weaire, Phys. Rev. Lett., **54**, 1392 (1985).

21. P. N. Keating, Phys. Rev., **145**, 637 (1966).

22. R. Car and M. Parrinello, Phys. Rev. Lett., **60**, 204 (1988).

23. R. Car and M. Parrinello, Phys. Rev. Lett., **55**, 2471 (1985).

24. R. Car and M. Parrinello, in Proc. 18th Int. Conf. Phys. Semicond., Stockholm, 1986, edited by Engston (World Scientific, Singapore, 1987), p. 1165.

25. W. A. Kamitakahara, H. R. Shanks, J. F. McClelland, U. Buchenau, F. Gompf, and L. Pintchovius, Phys. Rev. Lett., **52**, 644 (1984).

26. N. Maley, J. S. Lennin, and D. L. Price, Phys. Rev. Lett., **56**, 1720 (1986).

27. P. E. Meek, in "Physics of Noncrystalline Solids", edited by G. Frischat (Trans Tech, Aedemansdorf, Switzerland, 1977), p. 586.

28. D. Beeman, and R. Alben, Adv. Phys., **26**, 339 (1977).

29. W. A. Kamitakahara, H. R. Shanks, J. F. McClelland, V.Buchenau, F. Gompf and L. Pintschovius, Phys. Rev. Lett., **52**, 644 (1984).

30. D. Beeman, R. Tsu, and M. F. Thorpe, Phys. Rev. B, **32**, 875 (1985).

31. J. Fortner and J. S. Lannin, "Radial Distribution Function of Amorphous Silicon" (unpublished), The Department of Physics of Pennsylvania State University.

32. J. S. Lannin, J. Non-Crystallogr. Solids, **97 & 98**, 39 (1987).

CONCLUSIONS

The investigation of ZERODUR by high resolution solid state ^{29}Si and ^{27}Al NMR revealed the presence of two regions in the sample, one being highly ordered and the other relatively disordered. The ^{29} Si NMR spectrum showed clearly peaks and shoulders representing $Si(OAl)_n$ species in the ordered region. In the disordered region these peaks were inhomogeneously broadened, merged together and were not able to be separated. The Loewenstein rule was basically obeyed in both regions. The ^{27}Al NMR spectrum showed that the tetrahedral center of SiO_2 and AlO_2^- had near cubic symmetry in the ordered region, and axial symmetry in the disordered region. All Al Sites were tetrahedrally coordinated. No 5- or 6-coordinated Al sites were found in the sample.

High resolution solid state ^{29}Si NMR studies have also been performed on amorphous silicon films whose short range order has been modified. Measurements were made on low pressure rf sputtered a-Si deposited at room temperature and subsequently annealed to elevated temperatures. The NMR spectra under conditions of high resolution solid state NMR were a single broad line, whose second moment decreased upon annealing. The dominant contribution to the line width was associated with a broad distribution of isotropic chemical shifts. The variation of the NMR second moment with annealing temperature exhibited a monotonic decrease up to 610 °C, where an additional sharp line

associated with c-Si is observed. After annealing at 640 °C, the broad line disappeared, leaving only the sharp line. The changes in second moment with annealing were compared to recent data on the distribution function of two sputtered a-Si films whose bond angle deviation was known, as well as to Raman scattering measures of structural order. The results indicated that the NMR width variations were related to changes in the electronic states about Si sites and the associated narrowing of the bond angle distribution.

ACKNOWLEDGEMENTS

Among those who contributed to the completion of this work, I would particularly like to thank Marek Pruski and Dr. Bernard Gerstein.

I am also grateful to Qingxiao Ni for his assistance with EPR, Joe Harringa for X-ray work on amorphous Si, Dr. Shinar and Dr. Jeff Lennin for providing a-Si samples, Dr. Ann Nicol for providing aluminosilicate glass samples, and Dr. Fripiat's group of University of Wisconsin at Milwaukee for MAS NMR measurement of ^{27}Al of ZERODUR at 130 MHz.